ADVANCED ELECTRONIC MATERIALS
www.advelectronicmat.de

Transparent Electrodes for Efficient Optoelectronics

Monica Morales-Masis, Stefaan De Wolf, Rachel Woods-Robinson, Joel W. Ager, and Christophe Ballif**

With the development of new generations of optoelectronic devices that combine high performance and novel functionalities (e.g., flexibility/bendability, adaptability, semi or full transparency), several classes of transparent electrodes have been developed in recent years. These range from optimized transparent conductive oxides (TCOs), which are historically the most commonly used transparent electrodes, to new electrodes made from nano- and 2D materials (e.g., metal nanowire networks and graphene), and to hybrid electrodes that integrate TCOs or dielectrics with nanowires, metal grids, or ultrathin metal films. Here, the most relevant transparent electrodes developed to date are introduced, their fundamental properties are described, and their materials are classified according to specific application requirements in high efficiency solar cells and flexible organic light-emitting diodes (OLEDs). This information serves as a guideline for selecting and developing appropriate transparent electrodes according to intended application requirements and functionality.

1. Introduction

The past few years have witnessed an unprecedented entrance in both variety and volume of optoelectronic devices into the consumer-electronics market. With this growth, there has also been a transition to devices that offer attractive features such as semi-transparency, flexibility, stretchability, tactility, and energy efficiency. Most such devices with these attractive features require transparent electrodes that enable these functionalities. Sustainable fabrication of transparent electrodes with readily available raw materials and their recyclability are also important criteria for successful commercialization. This article reviews the status of the development of transparent electrodes for optoelectronic devices. In the first section, we list the relevant properties that these electrodes require for their intended applications, including transparency and conductivity. We also describe other factors that affect device operation or contribute to device efficiency. As an example, highly efficient silicon heterojunction solar cells can generate short-circuit current densities higher than 40 mA cm^{-2} that must be laterally transported to the metal contacts of the cells.[1] Such large photogenerated current densities require transparent electrodes that can carry the current densities over large surface areas without excessive power dissipation. The electrodes in some light-emitting diodes (LEDs) must also transport similarly large current densities. In the second part of this report, we describe the distinct material systems that simultaneously enable transparency and conductivity and that are available either at the laboratory or the commercial scale. In the third section, we classify transparent electrodes according to their applicability to various types of highly efficient solar cells and to organic and inorganic LEDs (OLEDs, LEDs). To this classification, we add the processing compatibility requirements for actual device fabrication and electrode integration. Because reviews on each class of transparent electrodes are available (e.g., on metal oxide electrodes for displays and thin-film transistors,[2,3] on properties of transparent conductive oxides (TCOs);[4–7] and on general properties of graphene, carbon nanotubes and metallic nanostructures[8]), the last section presents transparent electrodes by mostly focusing on the technological development, applications, and our perspective on future developments of inorganic electrodes.

Dr. M. Morales-Masis, Prof. C. Ballif
Ecole Polytechnique Fédérale de Lausanne (EPFL)
Institute of Microengineering (IMT)
Photovoltaics and Thin Film Electronics Laboratory
Rue de la Maladière 71, Neuchatel 2002, Switzerland
E-mail: monica.moralesmasis@epfl.ch;
christophe.ballif@epfl.ch

Prof. S. De Wolf
King Abdullah University of Science and Technology (KAUST)
KAUST Solar Center (KSC)
Thuwal 23955–6900, Saudi Arabia

Prof. J. W. Ager
Materials Sciences Division
Lawrence Berkeley National Laboratory
Berkeley, CA 94720, USA

Prof. J. W. Ager
Department of Materials Science and Engineering
University of California, Berkeley
Berkeley, CA 94720, USA

R. Woods-Robinson
Applied Science and Technology Graduate Group
University of California, Berkeley
Berkeley, CA 94720, USA

DOI: 10.1002/aelm.201600529

2. Application Requirements of Transparent Electrodes in Optoelectronic Devices

Typical optoelectronic devices that require transparent electrodes include touchscreens, liquid-crystal displays (LCDs), smart windows, most types of solar cells (e.g., thin-film silicon, chalcopyrite, organic, perovskite, and silicon-wafer-based

ADVANCED ELECTRONIC MATERIALS
www.advelectronicmat.de

ADVANCED SCIENCE NEWS
www.advancedsciencenews.com

heterojunction solar cells), OLEDs, and LEDs. In general terms, the electrodes in solar cells should simultaneously guarantee unhindered current flow out of a large device area and efficient light coupling into the active area of the cell.[9] Displays and OLEDs have very similar requirements for their electrodes: current flow in and light coupling out. It is therefore tempting to suggest that all optoelectronic devices have identical requirements in terms of optical transmittance-lateral conductivity properties.[10] However, optimal performance from each type of device can be achieved only by specific optimization of its electrodes, such as minimized contact resistance with the adjacent active layer of the device (e.g., by work function matching),[11–13] low-damage deposition processing,[14–16] conformal film deposition, stretchability and bendability,[17–19] or temperature stability. In this context, we present the main requirements for transparent electrodes in each type of device in **Table 1**.

We note that lateral conductivity is evaluated as sheet resistance ($R_{sh} = 1/\sigma d$, where σ is the electrical conductivity of the material and d is the thickness of the electrode). As a device-relevant parameter, R_{sh} is used for comparison of the transparent electrodes discussed in Section 4 rather than conductivity, which is an intrinsic material property. Because of the broadness of this topic, we hereafter narrow our focus to transparent electrodes for high efficiency solar cells, LEDs and OLEDs.

3. Material Systems for Transparent Electrodes

Only a few material systems simultaneously offer optical transparency and electrical conductivity. In fact, there is always a trade-off between these properties, which fortunately can often be tuned for specific applications. The first and most traditional strategy for developing a transparent conductor is to find a material that intrinsically offers both characteristics, i.e., a wide band-gap material with n- or p-type conduction. Classic examples of n-type doped transparent conductors are Sn-doped In_2O_3 (ITO), F-doped SnO_2 (FTO), doped zinc oxide (ZnO), and cadmium oxide (CdO).[4,22–25] Conductive polymers such as poly(3,4-ethylenedioxythiophene) doped with polystyrene sulfonic acid (PEDOT:PSS) also partially offer both intrinsic properties.[26–28] A second strategy consists of dimensional engineering using conductive, but not necessarily transparent materials (e.g., metals or carbon-based materials[29]) and their arrangement in such a way that the system conducts in one direction and is transparent in the other. This is achieved by arranging the conductive material in either a very thin layer or a mesh of (nano-)wires.[8,30–32] The use of 2D materials can be considered as a third approach, with graphene as the most prominent material.[33–35] The latter material offers in theory in-plane (ballistic) conductance, while being quite transparent due to their limited thickness. Also available are hybrid approaches that combine the properties of several material systems into a single functional electrode,[36–39] such as embedded metal nanowire networks in a dielectric matrix. Below, we consider three approaches that build on inorganic transparent electrodes developed in recent years, their fundamental properties, their fabrication processes, and their position in the market either as raw materials or utilized in commercial devices. To classify the electrodes based on its technology maturity we used the concept

Monica Morales-Masis is team leader for transparent electrodes development at the Photovoltaics and Thin-Film Electronics Laboratory (PVLab) of the Ecole Polytechnique Federale de Lausanne (EPFL), Switzerland. She obtained her Ph.D. in Physics from Leiden University, The Netherlands in 2012, focusing on resistive switching memories. Her current research interests include the design, synthesis, functionalization, characterization and fundamental investigation of novel materials for applications in optoelectronic devices, including solar cells and light emitting diodes.

Stefaan De Wolf received his Ph.D. degree in 2005 from the Katholieke Universiteit Leuven in Belgium, during which time he was also affiliated with imec in Belgium, working on crystalline silicon solar cells. From 2005 to 2008, he was with the National Institute of Advanced Industrial Science and Technology (AIST), Tsukuba, Japan, investigating silicon heterojunction structures and devices. In 2008, he joined the Photovoltaics and Thin-Film Electronics Laboratory, Ecole Polytechnique Federale de Lausanne (EPFL), Neuchatel, Switzerland, as a team leader for its activities on high-efficiency silicon solar cells. Since September 2016 he is associate professor at the King Abdullah University of Science and Technology (KAUST) in Saudi Arabia.

Rachel Woods-Robinson received her B.S. in Physics from UCLA, and is currently a Chancellor's Fellow and NSF Graduate Fellow Ph.D. student in Applied Science and Technology (AS&T) at UC Berkeley. She is conducting her thesis research at Lawrence Berkeley National Laboratory (LBNL) and the National Renewable Energy Laboratory (NREL), applying high-throughput materials computation, synthesis, and characterization to study materials for renewable energy and optoelectronic applications. She is the co-founder of Cycle for Science, a science education outreach organization, and is part of the 2016 inaugural class of the SHIFT Emerging Leaders Program in Jackson Hole, WY.

Table 1. General requirements of optoelectronic devices and their transparent electrodes.[2,8,20,21]

Transparent Electrode Requirements	Optoelectronic Device				
	Touch Screens	LCDs	Smart Windows	LEDs/OLEDs	Solar Cells
Sheet resistance (Ω sq^{-1})	300–500 (resistive touch panels) 100–1000 (capacitive touch panels)	100–300 (pixel, TFT) 30–80 (common LCD)		10–100	
Transmittance range (nm)	Visible (380–700 nm)		UV-vis-NIR	Visible (380–700 nm)	UV-vis-NIR
Other					
Uniformity	+++	+++	+++	+++	+++
Conformal coating	++	+++	+	+	+
Smooth surface	+++	++	+	Bottom- emitting: +++ Top-emitting: –	– (Haze beneficial for light in-coupling)
Bendability	+++ (for thin film devices fabricated on flexible substrates)				
Low contact resistance with metal	+	+++	+	+++	+++
Low contact resistance with active layer	+	+	+	+++	+++
Work function match	–	–	–	++	++
Synthesis temperature	(process and application specific)				
Chemical/environmental stability	+++	+++	+++	+++	+++

of technology readiness level (TRL). The TRL are given in a range from 1 to 9, with 1 being the lowest level of technology readiness (at the scientific study stage, observation of basic principles) and 9 the highest level (when a technology reaches commercialization). As commented above, **Table 2** focuses on inorganic materials, extensive reviews of the conductive polymer approach have previously been published.[26,28,40]

3.1. Transparent Conductors

3.1.1. N-Type Transparent Conductors

Highly doped (degenerate) metal oxides, commonly known as transparent conducting oxides (TCOs), are the most widely used and studied transparent electrodes to date. Conventional TCO materials are tin-, zinc-, cadmium- and indium-based oxides (SnO_2, ZnO, CdO, In_2O_3). Other reported materials with TCO properties include titanium oxide (TiO_2) and calcium aluminate ($12CaO{\cdot}7Al_2O_3$).[42,43] Conventional TCOs are binary systems, mainly polycrystalline in nature and doped with halides, group XIII, or XV elements,[6] almost always forming n-type semiconductors. Recently, multi-compound oxides (e.g., IGZO, ZTO, IZO),[44] aiming at improved mechanical properties and thermal stability due to their amorphous nature, have also been widely studied and have electrical properties that are often on par with their polycrystalline counterparts.[44,45]

The simultaneous ability of binary and multi-compound metal oxides to offer high optical transmittance in a broad photon-energy range and high electrical conductivity is attributed to their specific electronic structure. Conventional TCOs are mainly formed by metal atoms with the $(n-1)d^{10}ns$[2] electronic configuration.[44,46] Interaction of the metal s states (Ms) and oxygen p states (Op) results in the formation of a wide band gap ($E_g > 3$ eV), allowing the transmittance of photons in the visible range and below.[47] The valence band (VB) is composed of occupied oxygen 2p states, whereas the conduction band (CB) is formed by an overlapping Ms-Op-Ms network. This Ms-Op-Ms network results in a highly dispersed band (observed as a large curvature at the conduction band edge, see figure in Table 2, column 2, row 2) which leads to a low effective electron mass (m_e^*) in the range of $0.2–0.3m_0$, where m_0 is the resting mass of the electron.[48] The electron mobility (μ) in dispersed bands in the relaxation time approximation depends on m_e^* and the average time between two scattering events (or carrier relaxation time) (τ), according to the following expression:

$$\mu = \frac{e\,\tau}{m_e^*} \tag{1}$$

τ is influenced by all possible scattering mechanisms relevant to electron transport in the films: grain boundaries in polycrystalline materials,[49] microstructural defects such as voids or stacking faults, point defects such as neutral or ionized impurities and lattice vibrations (i.e., phonon scattering). To increase the free electron mobility in TCOs, a low m_e^*, low free-carrier density and low-defective material are thus required. Typical TCO electron mobilities range from 10 up to 200 cm^2 V^{-1} s^{-1}.[3] The electron mobilities of polycrystalline and amorphous TCOs can be very similar. This similarity is generally attributed to the spherical symmetry of the Ms orbitals, which has a marginal effect on the angular variations in the Ms-Op-Ms-network; this network forms the conduction band. The Ms-Op-Ms overlap (the cation-oxide orbital hybridization) plays a key

ADVANCED ELECTRONIC MATERIALS
www.advelectronicmat.de

Table 2. Types of transparent conductive electrodes. The properties that allow simultaneous transmittance and conductivity, i.e., wide band gap and degeneration conduction in n-type TCOs (first two rows in column 2), metallic conduction by percolation through sparse nanowire networks (first two rows in column 3), and ballistic transport in the specific case of a monolayer of graphene, allowing transparency because of its 1-atom thickness (row 2, column 4).[41] The materials and deposition techniques used to fabricate these transparent electrodes are listed along with their market readiness and estimated technology readiness level (TRL).

	TCOs	Metal NWs	2D materials
Description	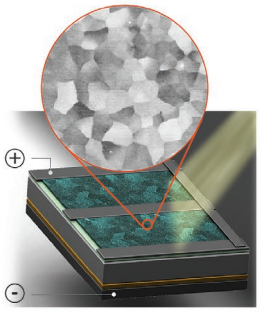	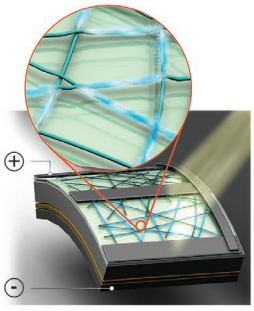	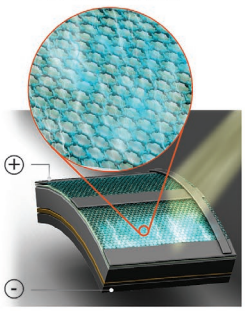
Band structure	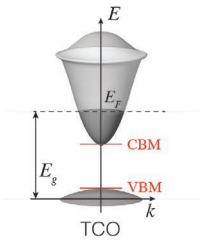 TCO E_F in CB: conductivity Band gap: transparency	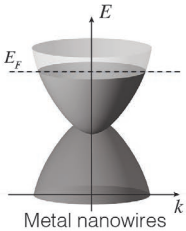 Metal nanowires Metal: conductor (no E_g) Small diameter and space between nanowires: transparency	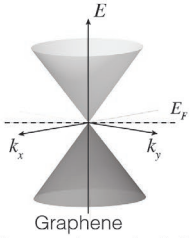 Graphene Ballistic transport: conductivity Atomic monolayer: transparency
Materials	In_2O_3, SnO_2, ZnO, CdO, TiO_2. Dopants: Sn, Ga, Al, B, H, W, Mo, Ce, F, Mg, Sb, In Multicompounds IGZO, IZO, ZTO, …	Ag, Cu, Au, Ni, Zn, C Hybrid electrodes: Ag NWs + PEDOT-PSS Ag NWs + metal oxides Ag NWs + graphene	C (graphene) Proposed alternatives: P,Sn,Si,Ge Hybrid electrodes: Graphene + PEDOT-PSS Graphene + metal oxides
Deposition	Sputtering (DC, RF) ALD APCVD LPCVD CBD PLD Spray Pyrolysis Spin Coating	Spray coating Drop-casting Slot Die on sheet or R2R	Mechanical exfoliation CVD on metal or BN substrates + exfoliation + film transfer.
Market	Widely used in an extensive number of devices.	In market, mainly as raw material. Limited number of devices.	In market, mainly as raw material for R&D labs. Limited number of devices.
TRL	4-9	3-8	1-6

Note:
E_g: optical band gap
E_F: Fermi level
CBM: conduction band minimum
VBM: valence band maximum

role in the electron transport in TCOs.[47,48,50] For example, cadmium oxide (CdO) features the largest electron mobility (in the range of 100–200 $cm^2\ V^{-1}\ s^{-1}$) in the TCO family.[47,51,52] This large mobility is attributed to the octahedral coordination of the oxygen atoms in the rocksalt structure of CdO. This octahedral coordination ensures a large Ms-Op overlap, which in

turn gives rise to a large dispersion of the conduction band and therefore a small m_e^*. Various types of indium-oxide-based TCOs also exhibit high electron mobilities, as discussed further in Section 4.

The electrical conductivity (σ) is proportional to μ and the free-carrier density (N_e) as $\sigma = e\mu N_e$. N_e can be increased in TCOs by doping; typically used extrinsic dopants are halides, group XIII and XV elements. Intrinsic dopants can also be used, with oxygen vacancies the primary example.[6] Intrinsically, the Fermi level (E_F) lies in most known TCOs close to the conduction band facilitating extrinsic n-type doping. Such doping shifts E_F inside the conduction band, forming a degenerate n-type semiconductor, which also leads to further widening of the optical band gap (E_g) following the Burstein–Moss relation: $\Delta E_g \approx N_e^{2/3}$.[5,53,54] Free-carrier densities of TCOs range from 10^{17} up to 10^{21} cm^{-3} (for comparison, metals have N_e on the order of 10^{22} cm^{-3}). Although increasing N_e can be beneficial to the optical transmittance in the UV-vis range (wider optical E_g), such an increase has negative effects in the NIR-IR part of the spectrum due to parasitic optical absorption by free carriers in the conduction band. This effect is called free carrier absorption (FCA), which is well described by the classical Drude theory.[55,56] The direct relation between the absorption coefficient (α) and N_e for the case of highly doped semiconductors is given by:[5,57]

$$a = \frac{\lambda^2 e^3 N_e}{4\pi^2 \varepsilon_0 c^3 n \left(m_e^*\right)^2 \mu_{opt}} \quad (2)$$

where λ is the photon wavelength, n is the refractive index, and μ_{opt} the optical mobility. It is important to note here that the μ_{opt} might differ from the Hall mobility (μ_{Hall}) since the former is not affected by macroscopic scattering effects as grain-boundaries or film dislocations. Therefore, in polycrystalline films, μ_{opt} is often referred as in-grain mobility.[56,58]

Equation (2) indicates that FCA ($A_{FCA} = 1 - e^{-\alpha d}$, with A the absorptance and d is the thickness of the film), will increase with N_e and d. To minimize FCA (a strict requirement for application in efficient solar cells), N_e should be reduced and μ maximized. The absorptance curves and their correlation with the electrical and microstructural properties of distinct TCOs are presented in Section 4 and Figure 2. A full derivation of Equation (2) is given in the Supporting Information.

3.1.2. P-type Transparent Conductors

All high-performance TCOs used in commercial applications are n-type. Comparable transparent p-type conductors have yet to be developed. If made available, they could be used in a number of applications, including as electrodes that could offer carrier selectivity and enable carrier collection in photovoltaic devices, as interconnect layers (i.e., recombination junctions) in tandem photovoltaics and as electrodes for fully transparent electronics. There have been some reports of transparent p-type conductors in the literature but their conductivities and figures of merit remain orders of magnitude lower than those of n-type TCOs (**Figure 1**). The difficulty in finding optimal p-type TCOs stems largely from the specific electronic structure of candidate wide-gap metal oxides, consisting of a highly localized oxygen 2p valence band with a large hole effective mass ($m_h^* > 1m_0$, compared with $0.2–0.3m_0$ for n-type) and thus a very low hole mobility, cf. Equation (1).[59] In addition, the valence band maximum (VBM) of most oxides is energetically situated deeply below the vacuum level, resulting in a high ionization potential. This impedes p-type doping, mainly due to compensation (i.e., "hole killing") by intrinsic defect generation of the intentionally introduced p-dopants.[60] To improve the mobility by achieving high crystal purity (and minimal scattering), most p-type TCOs, like their n-type counterparts, require high synthesis temperatures that jeopardize their use in devices with sensitive thermal budgets.

Fortunately, there are material design principles that can be employed to increase the mobility while maintaining wide optical band gaps in p-type metal oxides. The first such principle is to alloy a wide-gap metal oxide with Cu^{+1} to create $Cu_xM_yO_z$ and then to hybridize the Cu^{+1} closed-shell 3d[10] electrons with O2p orbitals. This approach, which delocalizes the valence band and thus decreases m_h^*, was used to demonstrate the first p-TCO, delafossite $CuAlO_2$, in 1997.[61] With a free carrier density of holes of $N_h = 1.3 \times 10^{17}$ cm^{-3} and a hole mobility at ≈10 cm^2 V^{-1} s^{-1}, the conductivity (<1 S cm^{-1}) was much lower than of n-type TCOs. Subsequently, other Cu-based delafossites with Al replaced by other metal cations, such as Cr,[62] Fe,[63] Sc,[64] and Y,[65] were investigated with oxygen intercalation and various synthesis methods (and thus, various microstructures) with the aim of decreasing the dopant compensation and increasing mobility (Figure 1). Recently, the $CuCrO_2$ has been explored with promising results; Mg-doped $CuCrO_2$ has the highest p-type conductivity reported for an oxide to date, 220 S cm^{-1}. In related work cationic and anion substitution and the role of Cr vacancies in this material has been studied.[66,67] High conductivity has also been shown experimentally in non-Cu metal oxides, most notably spinel-structured TCOs, such as $NiCo_2O_4$,[68,69] perovskites-structured TCOs, such as $SrIn_xTi_{1-x}O_3$ and $Sr_xLa_{1-x}CrO_3$,[70,71] and amorphous or composite oxides, such as $ZnO \cdot Rh_2O_3$ and In:MoO_3.[72,73] Other oxides, such as doped Cr_2O_3 and Ba_2BiTaO_6, have promise but remain to be synthesized with high conductivities.[74,75]

A second, more recently employed approach is to look beyond oxides. Interestingly, one of the first transparent conductors, discovered by Karl Baedeker in 1907, was a non-oxide, p-type degenerate semiconductor, CuI.[76,77] Non-oxide wide-gap (direct and indirect) semiconductors with P, S, or N anions are attractive candidates for p-type materials discovery as their valence bands are more delocalized, leading to a lower hole effective mass.[59,78] This approach has been demonstrated experimentally with Cu-based p-type transparent chalcogenides (S, Se, Te) and oxychalcogenides, most notably $CuAlS_2$, $BaCu_2S_2$, $BaCu_2$(S, Se)F, and Cu-Zn-S, resolving one of the issues with the localized O 2p orbital and, upon optimization, reaching conductivities greater than 10 S cm^{-1}.[79–82] The Cu-Zn-S system (also notated Cu_yS:$Cu_xZn_{1-x}S$) includes films grown at temperatures lower than 100°C by pulsed laser deposition (PLD) and chemical bath deposition (CBD), achieving p-type conductivities approaching those of the n-type TCOs (Figure 1).[82] Additionally, Hosono and co-workers have

ADVANCED ELECTRONIC MATERIALS
www.advelectronicmat.de

ADVANCED SCIENCE NEWS
www.advancedsciencenews.com

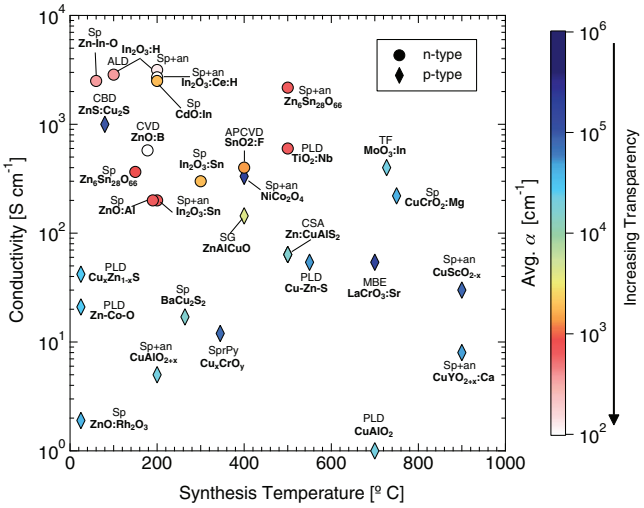

Figure 1. Conductivity in relation to synthesis temperature (or annealing temperature) for selected transparent n-type and p-type conductors reported in literature. The color bar represents the absorption coefficient (averaged from 400–700 nm), with white the lowest (most transparent) and blue the highest (least transparent). The synthesis method is listed above the compound name, where "Sp" is sputtered (DC or RF), "PLD" is pulsed laser deposition, "CVD" is chemical bath deposition, "APCVD" is atmospheric pressure CVD, "CBD" is chemical bath deposition, "SPS" is spark plasma sintering, "SG" is sol-gel, "SprPy" is spray pyrolysis, "TF" is tube furnace, and "+an" indicates an annealing step. Note that among all the n-type TCOs listed, only the TiO_2:Nb is not an s-band TCO, but a d-band TCO. A table with the complete list of transparent n- and p-type conductors and the respective references can be found in the Supporting Information.

developed a new class of transparent layered oxychalcogenides *Ln*OCu*Ch* (*Ln*: La, Pr, Nd, Sm, Gd, Y; *Ch*: S, Se), with conductivities up to 140 S cm^{-1}.[83,84]

The transparent conducting materials discussed above present different challenges in terms of optimization and eventual device implementation. The majority of oxide-based p-type conductors discussed have low carrier concentrations (10^{17} to 10^{19} cm^{-3}) and conduct via an activated transport or hopping mechanism. As a result, improving conductivity involves both increasing the electron density and the mobility. In the non-oxide chalcogenide-based systems, the band gap tends to be smaller compared to oxides. Additionally, the chalcogenide-based transparent p-type conductors are degenerately doped semiconductors with temperature-independent conductivity, limited by ionized impurity scattering. Compensation by deep donors can reduce both the hole concentration and the mobility, through the increase of ionized impurity scattering. This trade-off has been explored computationally for some specific oxide studies,[85,86] but a more general approach targeting non-oxides would be valuable. Phosphides and nitrides in general have lower hole effective masses, but are less transparent than oxides (phosphide band gaps are on the order of 2 eV).

To circumvent this trade-off, a third design principle, proposed by Varley et al., among others,[78] is to explore systems with a low m_h and a wide direct band gap. That is, materials with small indirect gaps could still be transparent in the visible so long as their direct gap is larger than 3.1 eV. Their study targeted and screened phosphides, suggesting further exploration of BP and AlP, among others. This approach was recently supported experimentally with pellets of CaCuP (with weak absorption at 2.2 eV and stronger absorption at 2.7 eV), showing conductivities up to 500 S cm^{-1}, although thin films of this material have yet to be synthesized.[87]

Figure 1 compares the conductivity of various high-performing transparent n-type and p-type conductors as a function of the synthesis temperature. It can be noted that at high values of conductivity the non-oxides tend to be more strongly absorbing due to their lower band gaps. Finally, as noted earlier, while n-type TCOs can reach high conductivity even in their amorphous state, p-type TCOs exhibit much lower conductivity at high synthesis temperatures.

3.2. Metal Nanowires, Nano- and Microgrids, and Ultrathin Films

The use of metal nanowires (NWs) as transparent electrodes is based on the high metallic conductivity of the wires. The nano-to-micrometer-scale diameters of these wires allow the formation of microscale network grids that are sufficiently sparse to avoid dramatic shadow losses in the transparency. As a consequence, the conductivity of such transparent electrodes does not depend on intrinsic materials properties, as is the case for TCOs, but rather on the network density, quality of the nanowires and optimum welding of the network interconnects. In detail, a high density of NWs limits transmittance by increased reflection in the visible. A high aspect ratio (long, small diameter) with good crystalline quality (defect-free to avoid electron scattering and no nanoparticle formation within the wire to avoid plasmonic absorption) and a highly pure metal lead to high-quality nanowires, and passage of electrical current without contact barriers comes from optimum welding of the network interconnects.[88] Silver (Ag) is the most commonly used metal for transparent electrodes due to its high conductivity. Cu and Zn, as well as carbon nanotube (CNT) networks, have also been widely proposed.[8,89] Usually, these networks can be deposited gently on underlying structures, which can be an advantage for processing-sensitive devices, such as organic[90] and perovskite solar cells.[91] Challenges common to all NW network approaches are their poor chemical stability and tendency to oxidize, their large surface roughness, their weak adhesion to the substrate and high contact resistance to adjacent functional layers in devices. To overcome some of these challenges, NWs can be embedded in transparent dielectrics, conductive polymers,[92] graphene oxide,[93] and metal oxides.[94] Stability data on NW electrodes are not widely reported, but recent efforts indicate possibilities to improve the performance of transparent NW electrodes. The properties of Ag NWs, CNTs, and several other nanostructures for applications as transparent electrodes, optimization approaches and performance have been extensively reviewed in ref. [8,89,95]

In relation to metallic networks, it is important to mention other recently proposed approaches. One consists of the formation of transparent conductive grid patterns by self-assembly of Ag nanoparticles deposited by ink-jet printing.[96] Another approach, closer to the standard one using macroscopic metal

grids, consists of 3D designs for the metal lines. These designs could redirect the light into the device avoiding shadow losses and forming "effectively transparent contacts".[97]

Ultrathin metal films have also been proposed as transparent conductors. Although these metal films have excellent electrical properties for thicknesses of only a few tens of nanometers, reflectance losses reduce the amount of light that couples effectively in devices, and the absence of a bandgap limits the transparency of the electrodes. Placing these metal films between two transparent, high-refractive-index layers reduces the reflectance of the metal, leading to gains in transmittance in the visible spectrum.[20] The optical absorptance and electrical properties of this type of electrodes are discussed in Section 4.

3.3. Graphene and Other 2D Materials

Two-dimensional (2D) materials have been widely proposed as transparent electrodes, due to their atomic monolayer thicknesses (allowing high optical transmittance) and the possibility of ballistic transport, i.e., non-scattering of electrons even at room temperature. Of these materials, graphene is arguably the leading 2D material, which, despite its lack of a bandgap, was also quickly proposed as a potential transparent conductor.[98,99] A monolayer of graphene can have carrier mobilities above 10 000 $cm^2\ V^{-1}\ s^{-1}$.[33] So far, such carrier mobility was achievable only in nanometer-scale, free-standing graphene flakes, obtained by mechanical exfoliation, and on films grown by chemical vapor deposition (CVD) on boron nitride substrates.[100] When transferring to substrates or upscaling the fabrication of graphene films, defects are introduced, thereby lowering the carrier mobility. Batch-to-batch production of high-quality graphene on large-area substrates, as well as the availability of transfer methods to obtain defect-free, high-quality graphene, remain major obstacles in the application of graphene to commercial optoelectronic devices.[101] Moreover, despite its high mobility potential, the conductivity of graphene is low compared with more conventional transparent electrodes, largely because of its intrinsically low free carrier concentration ($<10^{13}\ cm^{-3}$).[98] This may be resolved by impurity doping,[102] intercalation doping[103] and multilayer film growth,[33] all approaches that have resulted in device-relevant R_{sh} values. A clear advantage of graphene electrodes, like for metal NWs, is their tolerance to bending and stretching.[104] Therefore, for applications in which flexibility and stretchability are the most important requirements and a high R_{sh} is acceptable (e.g., foldable capacitive touch screens, see Table 1), graphene could be a good material candidate.

In addition to graphene, other emerging 2D materials such as phosphorene[105] and stanene (a single layer of Sn, yet to be experimentally realized) have been proposed as promising optoelectronic materials because of their potential to be as transparent and flexible as graphene.[106] Further exploration in this field could lead to 2D-layered materials with the performance required for use as transparent electrodes in flexible, deformable, or even skin-like optoelectronic devices.

Table 2 summarizes the above-described transparent electrodes, the property that allows both, conductivity and transmittance, the materials and methods used for fabrication, as well as their general position in the market.

4. Classification of Transparent Electrodes According to the Requirements for Solar Cells and OLEDs

The two most important requirements of a high-performance transparent electrode are low optical absorptance and high lateral conductivity (low R_{sh}). When comparing transparent electrodes, we should remember that optical properties are dependent on wavelength. It is precisely this dependency of the optical properties on wavelength that largely dictates which transparent electrode is best suited to a specific application. Materials that feature low absorptance in the wavelength range at which the active part of the device absorbs or emits light most efficiently should be explored. In this section, we classify various transparent electrodes according to their R_{sh} and optical absorptance using the following methodology: a) The optical absorptance of different electrodes is compared instead of the transmittance. The reason for this is that the often-used optical transmittance is strongly linked to the reflectance of the transparent electrode, which, in turn, is strongly influenced by the optical properties of the substrate, the film thickness, and the surface texture. In addition, while the transmittance is normally measured on a flat glass substrate, several solar cell absorbers feature textured surfaces (e.g., silicon heterojunction solar cells[1]) or randomly oriented grains (e.g., CIGS and CZTS[107]), which increase the roughness of the films and influence the reflectance of the layered stacks. To make an accurate and fair comparison of the amount of light that is parasitically absorbed by a transparent electrode, independent of the substrate and surface roughness, we therefore use the absorptance (A) value, defined as $A = 1 - TT - TR$, where TT is the total transmittance and TR is the total reflectance. b) The spectrally weighted absorptance ($A_{\text{weighted},x}$, where x is the solar cell or OLED) of the electrodes is compared rather than the absorptance at a single wavelength. The spectrally weighted absorptance takes into account the relevant wavelength range and the intensity of the light source that is absorbed or emitted by the device. This is expressed by

$$A_{\text{weighted},x} = \frac{\int_{\lambda_{1,x}}^{\lambda_{2,x}} I_{\text{light},x}(\lambda) A(\lambda) \mathrm{d}\lambda}{\int_{\lambda_1}^{\lambda_2} I_{\text{light},x}\, \mathrm{d}\lambda} \tag{3}$$

where $A(\lambda)$ is the absorptance of the transparent electrode as a function of wavelength, $I_{\text{light},x}$ is the intensity of the light source spectrum, and $\lambda_{1,x}$ and $\lambda_{2,x}$ are the wavelength's range as defined by the application. In solar cells, $I_{\text{light,solar}}$ is the 1 sun air mass 1.5 global (AM1.5G) solar spectrum. The wavelength range (λ_1 to λ_2) depends on the type of solar cell. Here, we use the wavelength range from $\lambda_1 = 320$ to $\lambda_2 = 1200$ nm (**Figure 2**a), which covers the range of most of the solar cells analyzed here. In OLEDs, $I_{\text{light,OLED}}$ is the emission spectrum of a white OLED in the wavelength range from $\lambda_1 = 380$ to $\lambda_2 = 780$ nm (**Figure 3**a). For display applications, the human optical

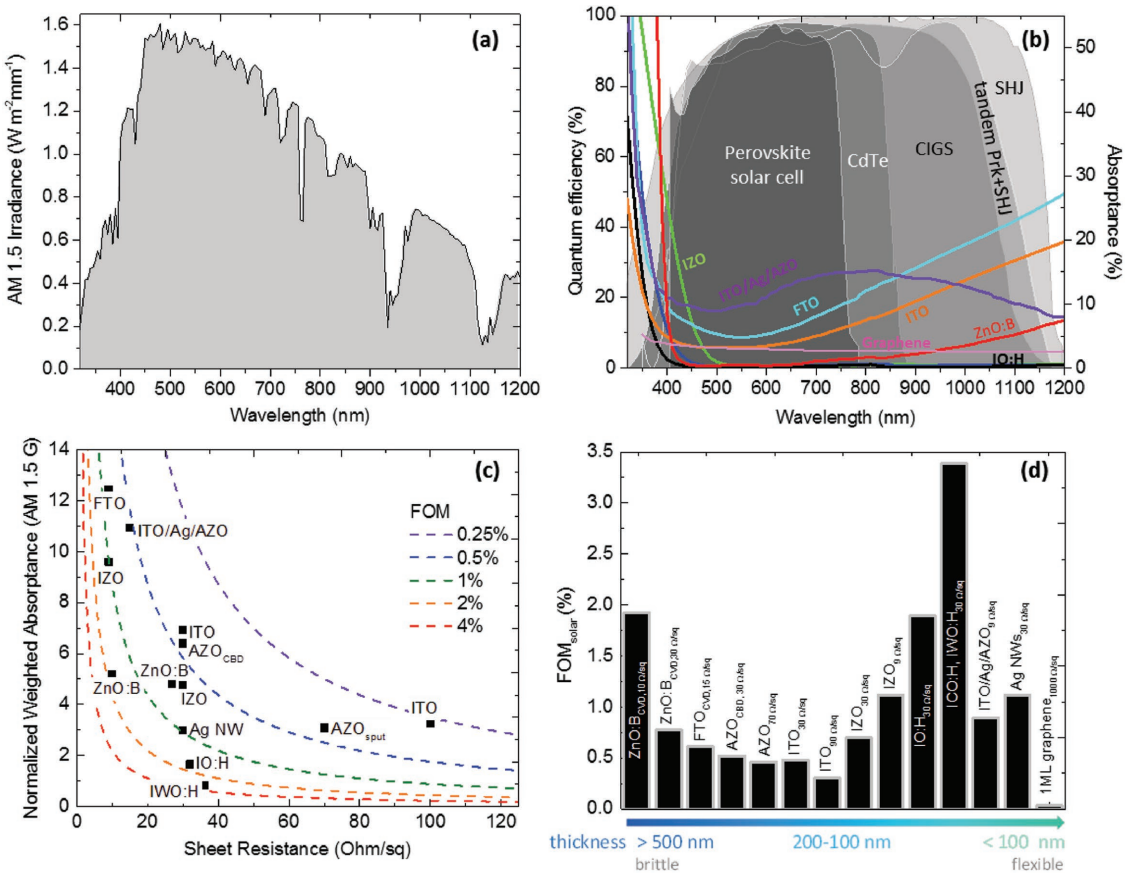

Figure 2. a) AM1.5G 1 sun irradiance spectra and b) quantum efficiency of a perovskite,[108] CdTe,[95] CIGS,[95] perovskite-SHJ tandem,[109] and SHJ[110] solar cells as a function of wavelength. The absorptance curve of different transparent electrodes measured on glass is also shown for comparison of the relevant wavelength range to be taken into account when developing transparent electrodes for solar cells. c) Weighted absorptance (calculated for the wavelength range from 320–1200 nm) in relation to sheet resistance for the compared transparent electrodes. The dashed lines indicate constant figure of merit (FOM) curves. d) FOM of transparent electrodes (Equation (4)) as a function of the thickness of the transparent electrodes. All the compared TCOs were deposited by sputtering deposition, with the exception of ZnO:B and FTO, which were deposited by CVD, and AZO_{CBD}, which was deposited by chemical bath deposition (CBD). All transparent electrodes were fabricated at temperatures lower than 200 °C to match the thermal budget of the solar cells.

sensitivity spectrum (Figure 3b) should also be taken into account. c) To compare different transparent electrodes, we use the following figure of merit (FOM):

$$\mathrm{FOM} = \frac{1}{A_{\mathrm{weighted},x} R_{\mathrm{sh}}} \tag{4}$$

As a result, high-quality transparent electrodes are characterized by high FOM values. d) Finally, with the exception of graphene, we compare transparent electrodes only for which transmittance and reflectance data have been reported.

4.1. Transparent Electrodes as Front Contacts in Solar Cells

Figure 2 shows the standardized terrestrial solar irradiance spectrum (AM1.5) under 1 sun intensity (a) and the external quantum efficiencies (QE) (left axis, b) for a range of archetypical high-efficiency solar cells that employ transparent electrodes, namely perovskite, copper indium gallium diselenide (CIGS), cadmium telluride (CdTe), silicon heterojunction (SHJ), and perovskite-SHJ tandem solar cells. The absorptance curves of various transparent electrodes are presented in Figure 2b (right axis).

Figure 2b shows that the front transparent electrode in any solar cell should have a sufficiently large (>3 eV) optical band gap to avoid absorption losses in the visible range of the spectrum. This requirement is already fulfilled by several TCOs.[23] For example, the optical band gap (E_g) of sputtered ITO, IZO and IO:H films are between 3.5 and 3.8 eV.[111] Transparent electrodes with low absorptance in the NIR-IR part of the spectrum (transparent electrodes with low FCA) are required for CIGS, SHJ and multi-junction devices, such as perovskite-on-silicon[109,112] and perovskite-on-CIGS[113] tandem solar cells, as these devices employ optical absorbers that are active in this range of the spectrum. These tandem approaches are new high-efficiency photovoltaic technologies, with a potential to reach about 30% efficiency,[114,115] clearly underscoring the critical importance and urgency of designing transparent electrodes with exceptionally large broadband transparency.

By comparing the absorptance curves of the TCOs in Figure 2b, we observe that hydrogen-doped In_2O_3 (IO:H)[116]

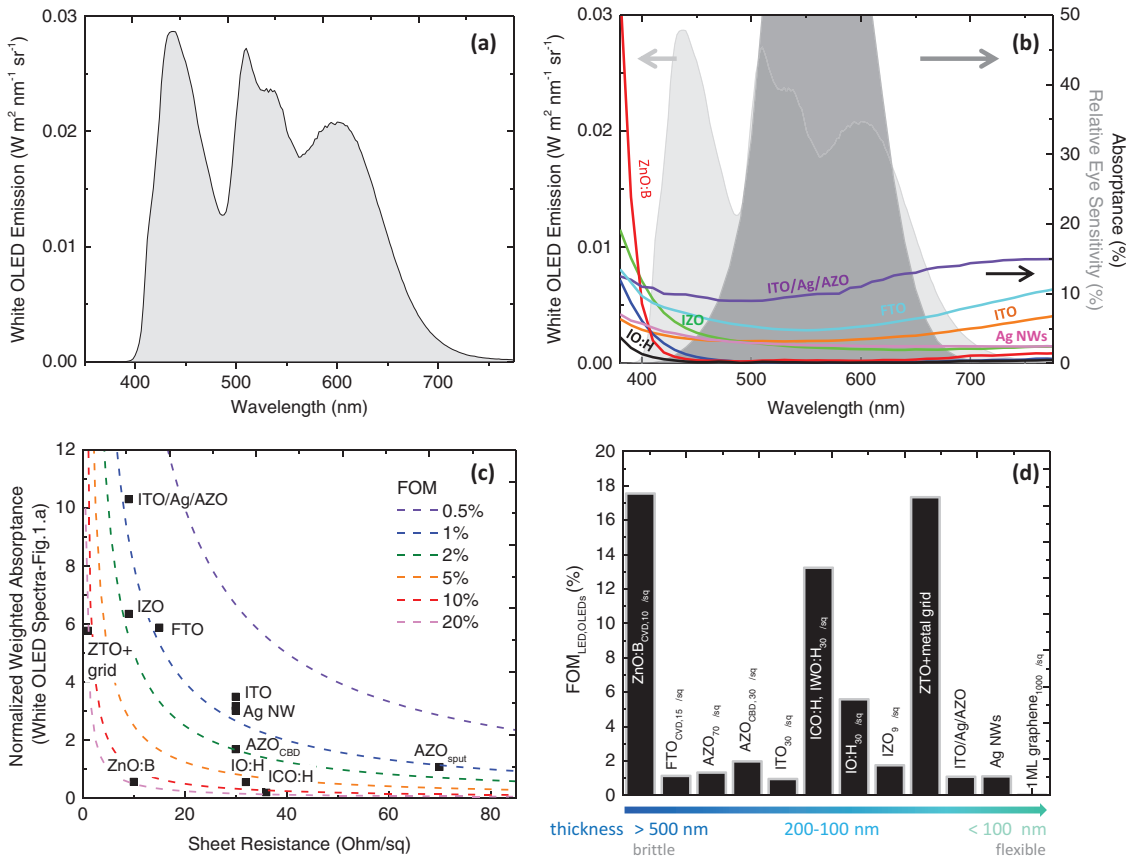

Figure 3. a) White OLED spectrum simulated with SETFOS (Fluxim AG)[155] as a function of emitted wavelength. b) Absorptance curves of different transparent electrodes (as measured on glass substrates) and the eye luminosity spectrum as an example of a relevant transmittance wavelength range for displays. c) Weighted absorptance (calculated from 380–780 nm) in relation to sheet resistance for the different transparent electrodes compared. The dashed lines indicate curves of constant figure of merit (FOM). d) FOM of transparent electrodes (Equation (4)) as a function of the thickness of the electrodes compared. All TCOs were deposited by sputtering deposition, with the exception of ZnO:B and FTO, which were deposited by CVD, and AZO_{CBD}, which was deposited by chemical bath deposition (CBD). All transparent electrodes were fabricated at temperatures lower than 200 °C, matching the thermal budget of flexible OLEDs.

and cerium/hydrogen or tungsten/hydrogen co-doped In_2O_3 (ICO:H, IWO:H, respectively)[117] offer the best optical properties, with an absorptance below 2% from 400 up to 1200 nm. Another notable TCO with minimal absorptance in the NIR-IR range is doped CdO[52] (not shown here). These TCOs have an excellent optical-electrical trade-off, potentially from their exceptionally high electron mobilities, on the order of 100–200 cm^2 V^{-1} s^{-1}, combined with their relatively low free carrier densities. More specifically, in the case of IO:H, ICO:H, and IWO:H, the free carrier densities are usually below 3×10^{20} cm^{-3}. Their electron mobilities are about 100 cm^2 V^{-1} s^{-1} for IO:H and IWO:H and 140 cm^2 V^{-1} s^{-1} for ICO:H, resulting in R_{sh} in the range of 30–40 Ω sq^{-1} (Figure 2c), which are excellent values for high-efficiency solar cell applications. The high free electron mobilities in these polycrystalline hydrogenated In_2O_3-based materials are explained by the formation of large grains, together with possible grain-boundary passivation by hydrogen, as well as the fact that H atoms in the film do not contribute significantly to ionized or neutral impurity scattering.[118,119] IO:H, ICO:H, and IWO:H have been successfully applied in SHJ,[117,120–122] CIGS,[123] and perovskite solar cells.[124]

Amorphous indium zinc oxide (IZO) is another TCO with low FCA and good electrical properties. Even with an amorphous structure (different from polycrystalline IO:H and ICO:H), IZO can have electron mobilities up to 60 cm^2 V^{-1} s^{-1} for free carrier densities between $1–3 \times 10^{20}$ cm^{-3}.[111,125,126] An attractive feature of these TCOs is that they already have excellent optoelectronic properties in their as-deposited state; these properties are not much affected by post-deposition annealing and offer opportunities for temperature-sensitive applications. A possible drawback is their relatively high absorption in the UV-vis range due to optical band gap narrowing.[111] This is a common effect in amorphous materials caused by exponential subgap tails due to disorder (also called Urbach tails)[127,128] and the presence of defects that introduce subgap absorption centers.[129] The application of IZO in solar cells has been demonstrated in SHJ[111] and perovskite solar cells.[130]

A particularly attractive feature of all indium-oxide-based electrodes (including ITO) is the fact that their refractive index is close to 2. This is approximately the geometric mean of the refractive indices of air and typical solar cell absorbers (such as silicon), which gives these materials very good anti-reflective coating (ARC) properties. To fulfill ARC conditions, the optically

ideal thickness is dictated by quarter wave-length conditions, corresponding to about 75 nm for the AM1.5G spectrum, ensuring a reflection minimum at 600 nm.

Boron-doped ZnO (BZO) has attractive properties for certain photovoltaic devices as well.[131–133] A BZO electrode with a sheet resistance of 30 Ω sq^{-1} essentially shows the same low NIR-IR absorptance as IO:H (30 Ω sq^{-1}), even though much thicker BZO films are required to obtain such results. Regardless of the thickness, BZO maintains its excellent optical properties for two reasons: low free carrier densities (in the order of 10^{19} cm^{-3}) and a particular increase of electron mobility with increasing film thickness (due to its pyramidal shaped grains).[134,135] Electron mobilities up to 58 cm^2 V^{-1} s^{-1} have been achieved in BZO films post-treated with H_2 plasma.[136] The red curve in Figure 2b shows the absorptance of a BZO electrode with 10 Ω sq^{-1} R_{sh}. This very low R_{sh} is achieved by increasing the thickness of the film by 1 to 5 µm. Given the required thickness to obtain sufficiently conductive films, BZO films are not used as antireflective coatings. However, due to their self-texturing tendency during CVD, they offer excellent light-trapping conditions for thin-film photovoltaics, as evidenced by their successful application in thin-film silicon[137,138] and CIGS solar cells.[139]

The absorptances of Sn-doped In_2O_3 (ITO) with 30 Ω sq^{-1}[111] and fluorine-doped SnO_2 (FTO) with 15 Ω sq^{-1}[140] are already much higher than those of IO:H, IWO:H, ICO:H, IZO, and BZO. The high parasitic absorption in the NIR range of these materials originates from their high free carrier densities, required because their electron mobilities are lower than 40 cm^2 V^{-1} s^{-1}. Current losses linked to parasitic absorption in the front ITO in SHJ cells or in the front FTO in perovskite-SHJ tandem cells have been analyzed in ref. [140] and ref. [141], respectively. The popularity of both TCOs for application as window layers in solar cells is partly due to their chemical and environmental stability, as well as their demonstrated large-scale production.[142,143] It is important to note that while IO:H and ICO:H are excellent electrodes for photovoltaic cells, they are still relatively new materials and their fabrication at production-relevant scales is yet to be demonstrated. One of the challenges for upscaling hydrogenated indium oxides is to control the introduction of water molecules during deposition (to include the H dopants). Approaches such as the use of atomic layer deposition (ALD) would be, for example, a controlled way to grow high mobility IO:H.[118] With the obvious efforts to replace ITO with high-mobility TCOs, we expect the development of industry-relevant techniques for their fabrication.

Aluminium-doped ZnO (AZO) electrodes have also been widely used in PV devices.[144–146] AZO, like BZO, is attractive due to its non-toxicity and the abundance of Zn in the Earth's crust. The low FOM value compared to, e.g., BZO, is due to the higher FCA in AZO. AZO is polycrystalline, with a columnar-like structure, forming grain boundaries that limit its mobility (typically on the order of 10–20 cm^2 V^{-1} s^{-1}). Post-thermal treatments are known to improve the resistivity of AZO by increasing its free carrier density.[147] The electron mobility of sputtered AZO has been successfully increased up to 40–67 cm^2 V^{-1} s^{-1} by incorporating a capping layer and applying a high-temperature (650°C) annealing step.[148] Considering the temperature restriction of several devices, low R_{sh} values are therefore mainly achieved by increasing N_e, at the cost of an inflated FCA. Although the FOM values for sputtered and chemical-bath-deposited (CBD) AZO are similar, deposition from solution presents some advantages: it is a simple and low-cost process,[149] and it is gentle, preventing physical damage to the substrates or active device layers where the material is deposited. Next to CBD, ALD and CVD are gentle deposition techniques as well and used for fabrication of several of the transparent electrodes discussed here.

The ITO/Ag/AZO layer stack suffers the highest absorptance, from 500 to 800 nm, of all the curves compared. This is related to large reflectance and absorption losses in the thin metal film that provides the very low R_{sh} values. The shown absorptance is from[150]; however, approaches to improve the optical properties, e.g., by oxidizing the intermediate Ag film, have been demonstrated in subsequent reports.[151] While these films are not optimal for high efficiency solar cells, the possibility of sputtering these layers at room temperature, the limited total thickness of the trilayer-stack (<100 nm) and the ductility of the intermediate metal layer, with a thickness between 8 and 12 nm, make these electrodes interesting for flexible optoelectronic devices. Additionally, the high reflectance of these layers has been used to create a resonant optical cavity to trap the light in organic solar cells and, as a consequence, to increase their quantum efficiencies.[152] A summary of the approaches to optimize these types of dielectric/metal/dielectric layers for application in organic photovoltaic devices is found in ref. [153].

Finally, the absorptance curve of a monolayer of graphene, as reported in ref. [41], indicates that the use of such a material can be beneficial for applications in the NIR-IR range. However, in the visible range, the absorptance is already much higher than several of the other shown transparent electrodes. This is also reflected by the fact that a realistic R_{sh} value of 1000 Ω sq^{-1}[154] results in the lowest solar-cell FOM of all transparent electrodes, as shown in Figure 2d, casting doubt on whether monolayer graphene will ever find applications in highly efficient solar cells. As noted earlier, doping approaches and multilayers of graphene reduce the R_{sh} to more device-relevant values, but this is at the expense of increased absorptance.[41]

Figure 2c shows normalized weighted absorptance as a function of R_{sh} for the various transparent electrodes compared here. Dashed lines of constant FOM are given for reference. These dashed lines highlight the observation that FOM converges for cases of very large R_{sh} values with very low absorptance or vice versa. Therefore, in Figure 2c we restricted the comparison of FOM values for transparent electrodes to a maximum of R_{sh} = 100 Ω sq^{-1}, which is a relevant value for applications in photovoltaic devices.

Figure 2d compares the FOM of transparent electrodes classified by thickness. The electrodes are sorted from left to right with the thickest electrodes, poorly suited for flexible applications on the left, and thinner electrodes, which present higher resistance to mechanical bending and stretching, on the right.[18]

Note that Figure 2 considers a very general case by using only the AM1.5G solar irradiance spectrum under a 1 Sun intensity to evaluate transparent electrodes for any solar cell. To calculate the FOM for a specific solar cell, Equation (3) can be modified to include the quantum efficiency of the device:

$$A_{\text{weighted},x} = \frac{\int_{\lambda_{1,x}}^{\lambda_{2,x}} I_{\text{light}}(\lambda) QE(\lambda) A(\lambda) \mathrm{d}\lambda}{\int_{\lambda_{1,x}}^{\lambda_{2,x}} I_{\text{light}} QE(\lambda) \mathrm{d}\lambda} \quad (5)$$

4.2. Transparent Electrodes as Front Electrodes in OLEDs

To evaluate FOM of transparent electrodes geared towards applications in OLEDs (a similar case would apply for bottom-emitting LEDs), we use a white OLED spectrum simulated with SETFOS.[155] Figure 3 shows the white OLED spectrum used as I_{light} (λ) in Equation (4) to evaluate the weighted absorptance of transparent electrodes. Contrary to solar cells, applications in LEDs, or OLEDs for lighting, displays or touch screens feature a narrower wavelength range at which the transparent electrode should have minimum absorptance, relaxing the optical requirements as compared with solar cells. In fact, effects such as the Burstein-Moss shift or FCA in TCOs have only a minimal influence on the parasitic absorption for these applications. Nevertheless, we can observe in Figure 3b that the absorptance of the TCOs still follows a similar trend as in Figure 2b,c, with ZnO:B, ICO:H, and IWO:H the transparent electrodes with the lowest absorptance and highest conductivity, and therefore exhibiting the highest FOMs. In this comparison, we have also included the case of a zinc tin oxide (ZTO) combined with metal grids embedded on a polymer matrix.[156] ZTO is an amorphous TCO, with sufficient conductivity to be utilized in combination with metal grids as the anode in large-area flexible OLEDs. In fact, it was demonstrated that with the same type of metal grids, ZTO devices performed better than the reference ITO OLEDs.[157]

As observed in Figure 3c, the combination of the exceptionally low absorptance and a R_{sh} of 10 Ω sq^{-1} for ZnO:B, or even a lower R_{sh} (1 Ω sq^{-1}) provided by the metal grids in the case of the hybrid ZTO + metal grid electrode, gives the highest FOM to these two transparent electrodes. The large thickness of ZnO:B, required to achieve low R_{sh} values, may prevent its application in flexible devices, however, as indicated in Figure 3d. For such applications, hybrid electrodes based on ZTO and metal grids may offer a better alternative.[156] However, in rigid top-emitting LEDs, ZnO:B, when grown by LPCVD, has the additional advantage of an intrinsic pyramidal surface texture with known light scattering properties,[137] improving light out coupling.[158]

TCO/metal/TCO stacks and Ag NWs are on par in our FOM comparison. Although neither features simultaneously optimal R_{sh} and absorptance, these transparent electrodes offer properties that are interesting for flexible devices. For our comparison, we use representative absorptance and R_{sh} data of Ag NWs taken from the current literature.[8,95,159,160] However, we note that intensive research efforts are ongoing on Ag NWs, promising further performance improvements. Such improvements will mainly be achieved by increased fabrication control and deposition of metal grids with submicron-width lines,[161] development of hybrid approaches to improve stability under corrosive and oxidation conditions, as well as improved adhesion to the substrates.

A monolayer of graphene with a sheet resistivity of 1000 Ω sq^{-1} gives, by far, the lowest FOM for photovoltaics. We note that for the case of OLEDs, the FOM is reaching a comparable value relative to other transparent electrodes in the list. This is because the absorptance values of the various transparent electrodes are comparably low in the relevant wavelength range for these devices (the visible light spectrum). Nevertheless, the 1000 Ω sq^{-1} R_{sh} associated with a monolayer of graphene raises the concern of high resistive losses when applied in devices. Hybrid approaches offer help in such cases. As an example, several laboratory-scale OLEDs and LEDs have used graphene-based electrodes, i.e., hybrid nanowires and graphene, conductive polymer and graphene and graphene oxide layers.[35,162] However, only a few groups have demonstrated the use of a single layer of graphene as the anode in small-area OLED devices.[163]

5. Other Specific Requirements of Transparent Electrodes for Solar Cells and OLEDs

5.1. Fabrication Compatibility

As listed in Table 1, fabrication compatibility, i.e., processing temperature, chemical inertness, and non-damaging methods, is also an important selection criterion for transparent electrodes to be used in specific devices. For example, the thermal budget of OLEDs, SHJ, CIGS, CdTe, and perovskite-based solar cells is below 200 °C.[164,165] Clearly, fabrication of transparent electrodes on plastic flexible substrates also requires strict fabrication temperatures below approximately 150 °C. In this context, all electrodes depicted in Figure 2 and 3 were fabricated at temperatures lower than 200 °C, during both deposition and post-deposition annealing (when applicable). The only exception is FTO, which is normally deposited or post-treated at temperatures well above 200 °C.[166–168] Amorphous TCOs such as IZO, offer the greatest flexibility, as they can be deposited nominally at room temperature and do not require post-deposition annealing. Such TCOs have demonstrated their value in SHJ and perovskite solar cell fabrication.[111,130]

As mentioned earlier, gentle deposition on underlying layers can also be a critical factor in electrode choice and raises questions about the use of well-established physical vapor deposition (PVD) techniques, such as sputtering or pulsed laser deposition for certain applications. Sputter damage, caused by UV radiation and particle bombardment, is a known phenomenon in organic,[16] SHJ,[15] and perovskite[169] solar cells as well as flexible displays. Solutions to overcome such damage include the use of remote plasma sources,[170] the use of gently deposited buffer layers[171] or further improvements to solution-based deposition processes to improve the density and purity of TCO films to achieve high electron mobilities at low temperatures.[45,172]

5.2. Interfaces with the Transparent Electrodes

Good electrical and chemical matching at the interface between transparent electrodes and their adjacent layers in a device is another criterion for electrode selection and optimization. This interface can be shared with the carrier-collection or carrier-injection layers, but also with the metal grid of the device.

ADVANCED ELECTRONIC MATERIALS
www.advelectronicmat.de

ADVANCED SCIENCE NEWS
www.advancedsciencenews.com

Large-area optoelectronic devices often require a metal grid, which is normally deposited on the transparent electrode, to minimize the lateral resistance and, thus, voltage loss over large areas. As an example, we present a sketch of a cross section of a SHJ solar cell in **Figure 4** to highlight the hydrogenated amorphous silicon (a-Si:H)/TCO/metal interfaces with the corresponding band diagram. Transversely, minimizing electrical losses is equally important. Again, in SHJ solar cells, the main contributors to such transverse resistance are the contact resistances (ρ_c) at the metal/TCO interface (label **1** in Figure 4b) and, even more so, at the TCO/a-Si:H interface (label **3** in Figure 4b); the intrinsic resistance of the TCO in the transverse direction (label **2** in Figure 4b) is usually sufficiently low to be neglected.

Across the metal/TCO interface, the dominant carrier transport mechanism is field emission, for which the contact resistivity (ρ_c) is expressed as

$$\rho_c \propto \exp\left(\frac{\phi_B}{E}\right) \text{with } E = \frac{qh}{4\pi}\sqrt{\frac{N_e}{m^* \varepsilon_0 \varepsilon_\infty}} \text{ (field emission)} \quad (6)$$

where ϕ_B is the barrier height and E is the tunneling energy.[174] This equation makes evident the improvement in ρ_c from the increased carrier density, N_e, of the transparent electrode, which suggests the use of bilayer TCOs that feature high surface but low bulk N_e to minimize ρ_c and FCA simultaneously.[121]

Practically, the TCO/metal contact resistance is commonly characterized by the transfer length method (TLM).[175] In terms of metallization, screen-printed, low-temperature Ag pastes are commonly used, especially in industry. In such a case, ρ_c values on the order of 10^{-5} Ω cm[2] are typical, as is the case of the ITO/Ag and *a*-IZO/Ag interfaces, commonly used in solar cells.[111,176] Electroplated Cu can offer advantages in terms of line resistivity and material cost compared with printed Ag electrodes. However, due to the ease of diffusing electroplated Cu into silicon, where it can act as a carrier lifetime killer, its application to photovoltaics is not evident. Interestingly, ITO forms an excellent Cu diffusion barrier. The low measuredρ_c value for the Cu/ITO interface ($\rho_c < 10^{-4}$ cm^{-3}) validates this combination for high-efficiency silicon solar cells.[176] Contrary to the case of TCOs, achievement of sufficiently low ρ_c between the metal and Ag NWs or graphene electrodes is still an unresolved challenge.[100]

To extract or inject carriers efficiently in solar cells or OLEDs, respectively, the interface between the transparent electrode and the active layer of the device (absorber or emitter) should have a negligible contact resistance (ρ_c) as well.[177] A main cause of this resistance is the combined effect of Fermi-level pinning at the interface and work function mismatch between adjacent materials.[177] This causes the formation of an interfacial energy barrier, characterized by a certain height and depletion width penetrating both materials. Such barriers can in principle be overcome by thermionic (field) emission, evidenced by lowered ρ_c values with increasing operating temperatures.[178] The barrier width can also be narrowed by increasing surface doping to increase field emission across the interface, similar to the metal/TCO case. As an alternative to doping, the work function of TCOs can be modified by surface treatments (UV, ozone, oxygen plasma),[179] or by the application of specific interfacial buffer layers with optimized work functions. The work function and band alignment of various TCOs for selected devices have been studied by Kelvin probe microscopy (KPM) and X-ray photoelectron spectroscopy (XPS).[11,12,180] A selected list of TCOs and metals with their respective work function values as reported in literature is found in the Supporting Information (Table S2).

In metal NWs and graphene electrodes, the work function cannot be intrinsically modified; however, a common approach is the application of a capping layer or creating hybrid electrodes with high or low work function polymers[177] or metal oxide films.[181,182]

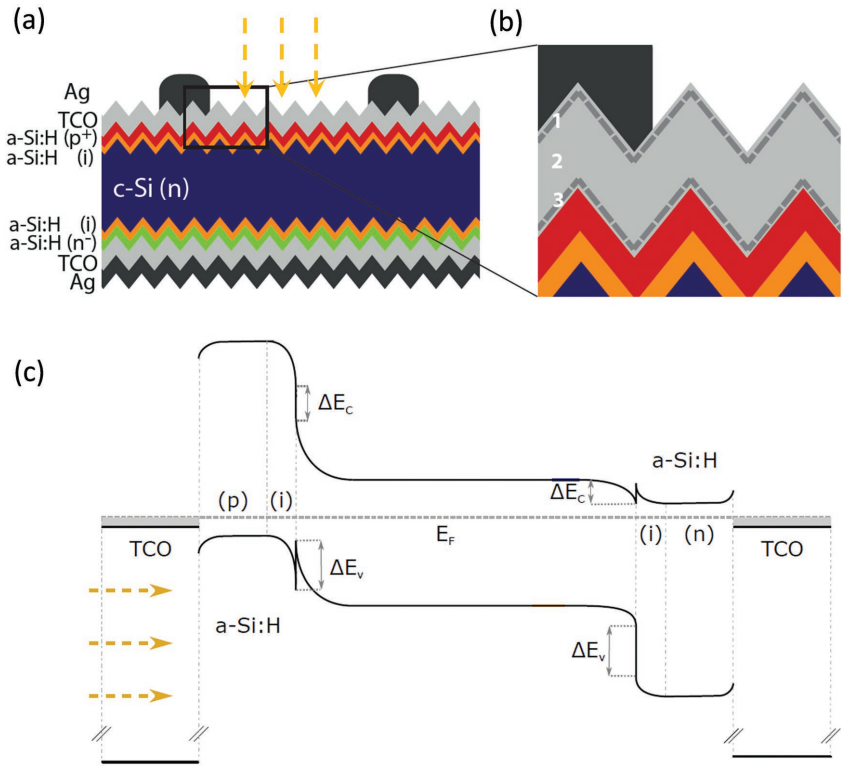

Figure 4. a) Silicon heterojunction (SHJ) solar cell structure and b) zoom-in of the front TCO layer indicating the 1. metal/TCO interface, 2. bulk and 3. TCO/a-Si:H(p) interface. c) Energy band diagram of a complete SHJ solar cell in equilibrium, showing the band structure between the c-Si/a-Si:H(p)/TCO at the front and c-Si/a-Si:H(n)/TCO at the back of the cell, acting as the hole and electron contact, respectively. In either case, collected carriers need to overcome in principle several barriers, namely at the c-Si/a-Si:H, the a-Si:H/TCO, and the TCO/metal interface (not drawn). The first barrier is caused by band offsets. The second one can be caused by Fermi-level pinning at the interface and insufficient doping of a-Si:H and TCO. Because the TCO is normally n-type, an Ohmic contact for electrons is in principle guaranteed on the rear side. Transport at the TCO(n)/a-Si:H(p) interface occurs by band-to-band tunneling with photogenerated holes efficiently recombining with electrons from the TCO.[173]

5.3. Stability Under Thermal and Humid Environments

Environmental stability of transparent electrodes is also of critical importance when integrating them in devices. Damp heat tests performed under standard conditions of 85% humidity at 85°C for prolonged time (1000 h) were used to demonstrate the high environmental stability of ITO and IZO electrodes.[183] IO:H and AZO, on the contrary, showed poorer electrical stability under damp heat conditions mainly due to the introduction of water at grain boundaries.[183,184] In the case of IO:H it has been recently demonstrated that damp heat degradation is strongly linked to the hydrogen content in the films. IO:H films with hydrogen content lower than 5 at.% exhibit stable electrical properties after exposure to DH conditions.[185] The application of capping layers, e.g., capping IO:H with a very thin and dense layer of ITO, improves the environmental stability of the electrodes.[183]

In terms of thermal stability, full-device fabrication might require temperature steps that could modify the carrier density or microstructure in TCOs, degrading the optoelectronic properties. TCOs with good temperature stability are mainly multi-compound amorphous materials, such as IZO and ZTO.[125,186] In nanowire networks, clustering of the network due to a temperature step would increase the roughness of the electrode and induce the formation of shorts in e.g. organic devices. In addition to temperature, UV exposure may also detrimentally affect some transparent electrodes. Conductive polymers used in organic devices and hybrid electrodes, such as nanowire-based and metal grids embedded in a conductive polymer, yellow with exposure to UV and temperature.[187] In terms of chemical stability, cleaning of the substrate before OLED or perovskite cell deposition can cause damage to the transparent electrodes. SnO_2, ITO, and a-ZnSnO are among the TCOs with the highest chemical stabilities[146] and therefore are fully compatible with industry-based processes to fabricate, e.g., OLED devices.[157]

6. Perspectives

The continuous drive to increase solar cell efficiency, as well as the push for improved performance of several other optoelectronic devices, requires the development of transparent electrodes with next-generation requirements, including ultrahigh broadband transparency, high conductivity, adaptability, and composition mainly from abundant elements. The best example of a device that requires premium broadband transparent electrodes on its front is the perovskite-silicon multi-junction solar cell, which, as indicated in Figure 2, aims at active absorption of the broadest photon-energy range. The electrodes in this type of solar cell need to feature a wide band gap, low FCA, and relatively low sheet resistivity. In addition, they should be deposited without damaging the carrier-selective contacts in the silicon cell, or the perovskite layers, and cannot be annealed. The best solution for this is a very high mobility TCO, deposited at room-temperature using a gentle deposition technique. Amorphous indium-based TCOs are the best candidates; however, widening of their band gap remains a challenge. Further exploration of materials to find the right dopants or compounds that open up the band gap or of new material systems with tuned compositions and microstructures is just one path to the discovery of amorphous low-temperature and gently-deposited high mobility broadband transparent electrodes.

In terms of deposition, further development of high-end deposition techniques, such as ALD, low-temperature solution-based deposition processes, or new PVD system designs that avoid the direct exposure of the substrate to the plasma during deposition (e.g., high-density plasma-enhanced evaporation,[188,189] or facing target sputtering[190]), is just one path to the development of ultra-high performance TCOs and TCOs/device interfaces.

Material design is also expected to play a decisive role in the development of Earth-abundant transparent electrodes, as well as for the discovery of high-performance transparent and conductive materials especially with p-type conductivity. Much is expected from high-throughput screenings using the combination of computational and experimental methods, looking for new design principles and experimenting with various synthesis approaches.

On the p-type TCO side, recent investigations of metal-based oxysulfides or non-oxide chalcogenides (S, Se, Te) or pnictides (N, P) as potential p-type transparent conducting candidates show promise in reducing the hole effective mass and to increase conductivity. Recent progress on sulfide-based p-type transparent conductors has enabled device demonstrations that employ p-type transparent contacts. For example, low-temperature synthesized Cu-Zn-S has been applied as a hole-selective contact in solar cells with n-type absorbers.[81] The scalability and low processing temperature of these p-type transparent conductors merits further material and device exploration.

Aside from transparency and conductivity, other specific properties (stretchability, self-healing, antibacterial properties) of transparent electrodes are becoming increasingly important as they are being implemented into thin, lightweight and wearable devices that require both ease-of-use and robustness. Examples of these are fiber-like electrodes,[191,192] consisting of fully integrated conductive fibers with a transparent matrix or skin-integrated circuits and optoelectronics that require transparent electrodes fabricated with non-toxic and biocompatible materials. The combination of optoelectronic and environmental or mechanical requirements is in many cases best achieved by hybrid approaches that integrate polymers and high-performance inorganic semiconductors. Lastly, in addition to the three different approaches to create transparent electrodes presented earlier in the manuscript, a largely unexplored area is the use of photonic crystals and metamaterials. In this case, light management through structures with metallic conductivity could simultaneously provide transparency and charge transport, creating transparent conductive structures.

Supporting Information

Supporting Information is available from the Wiley Online Library or from the author.

Acknowledgements

Part of this work was supported by the Swiss National Science Foundation (SNF), International co-operation program –ISV- Project

number IZK0Z2_171115; CCEM CONNECT PV; CTI FlexOLED and SNF Sinergia DisCO. J.W.A. was supported by the Electronic Materials Program, funded by Director, Office of Science, Office of Basic Energy Sciences, Materials Sciences and Engineering Division of the U.S. Department of Energy under Contract No. DE-AC02–05CH11231. S.D.W. was supported by funding from King Abdullah University of Science and Technology (KAUST). R.W.R. was funded by the National Science Fundation (NSF) Graduate Research Fellowship Program (GRFP) and by the UC Berkeley Chancellors Fellowship. The authors thank Virginia Unkefer from King Abdullah University of Science and Technology (KAUST) for manuscript editing, Heno Hwang, scientific illustrator from KAUST, for creating the illustrations in Table 2, Quentin Jeangros for the TCO SEM image and Jean Cattin for the energy band diagram, both from EPFL.

Received: December 7, 2016
Revised: January 18, 2017
Published online:

[1] C. Battaglia, A. Cuevas, S. De Wolf, *Energy Environ. Sci.* **2016**, *9*, 1552.
[2] X. G. Yu, T. J. Marks, A. Facchetti, *Nat. Mater.* **2016**, *15*, 383.
[3] T. Kamiya, H. Hosono, *NPG Asia Mater.* **2010**, *2*, 15.
[4] K. Ellmer, *Nat. Photonics* **2012**, *6*, 809.
[5] K. L. Chopra, S. Major, D. K. Pandya, *Thin Solid Films* **1983**, *102*, 1.
[6] S. C. Dixon, D. O. Scanlon, C. J. Carmalt, I. P. Parkin, *J. Mater. Chem. C* **2016**, *4*, 6946.
[7] E. Fortunato, D. Ginley, H. Hosono, D. C. Paine, *MRS Bull.* **2007**, *32*, 242.
[8] D. S. Hecht, L. B. Hu, G. Irvin, *Adv. Mater.* **2011**, *23*, 1482.
[9] J. Muller, B. Rech, J. Springer, M. Vanecek, *Sol. Energy* **2004**, *77*, 917.
[10] M. W. Rowell, M. D. McGehee, *Energy Environ. Sci.* **2011**, *4*, 131.
[11] A. Klein, C. Korber, A. Wachau, F. Sauberlich, Y. Gassenbauer, S. P. Harvey, D. E. Proffit, T. O. Mason, *Materials* **2010**, *3*, 4892.
[12] A. Klein, *J. Am. Ceram. Soc.* **2013**, *96*, 331.
[13] Y. H. Zhou, C. Fuentes-Hernandez, J. Shim, J. Meyer, A. J. Giordano, H. Li, P. Winget, T. Papadopoulos, H. Cheun, J. Kim, M. Fenoll, A. Dindar, W. Haske, E. Najafabadi, T. M. Khan, H. Sojoudi, S. Barlow, S. Graham, J. L. Bredas, S. R. Marder, A. Kahn, B. Kippelen, *Science* **2012**, *336*, 327.
[14] R. Wendt, K. Ellmer, K. Wiesemann, *J. Appl. Phys.* **1997**, *82*, 2115.
[15] B. Demaurex, S. De Wolf, A. Descoeudres, Z. C. Holman, C. Ballif, *Appl. Phys. Lett.* **2012**, *101*.
[16] H. Schmidt, H. Flugge, T. Winkler, T. Bulow, T. Riedl, W. Kowalsky, *Appl. Phys. Lett.* **2009**, *94*.
[17] Y. Leterrier, L. Medico, F. Demarco, J. A. E. Manson, U. Betz, M. F. Escola, M. K. Olsson, F. Atamny, *Thin Solid Films* **2004**, *460*, 156.
[18] Y. Leterrier, *Mechanics of Curvature and Strain in Flexible Organic Electronic Devices* (ed: Stergios Logothetidis), in *Handbook of Flexible Organic Electronics: Materials, Manufacturing and Applications*; Woodhead Publishing Ltd, Cambridge, UK **2015**.
[19] G. A. Salvatore, N. Munzenrieder, T. Kinkeldei, L. Petti, C. Zysset, I. Strebel, L. Buthe, G. Troster, *Nat. Commun.* **2014**, *5*.
[20] C. G. Granqvist, *Sol. Energy Mater. Sol. Cells* **2012**, *99*, 1.
[21] D. A. Jacobs, K. R. Catchpole, F. J. Beck, T. P. White, *J. Mater. Chem. A* **2016**, *4*, 4490.
[22] T. Minami, *Semicond. Sci. Technol.* **2005**, *20*, S35.
[23] S. Calnan, A. N. Tiwari, *Thin Solid Films* **2010**, *518*, 1839.
[24] H. Y. Liu, V. Avrutin, N. Izyumskaya, U. Ozgur, H. Morkoc, *Superlattices Microstruct.* **2010**, *48*, 458.
[25] D. S. Ginley, C. Bright, *MRS Bull.* **2000**, *25*, 15.
[26] M. E. Abdelhamid, A. P. O'Mullane, G. A. Snook, *RSC Adv.* **2015**, *5*, 11611.
[27] X. Crispin, F. L. E. Jakobsson, A. Crispin, P. C. M. Grim, P. Andersson, A. Volodin, C. van Haesendonck, M. Van der Auweraer, W. R. Salaneck, M. Berggren, *Chem. Mater.* **2006**, *18*, 4354.
[28] M. Vosgueritchian, D. J. Lipomi, Z. A. Bao, *Adv. Funct. Mater.* **2012**, *22*, 421.
[29] M. F. L. De Volder, S. H. Tawfick, R. H. Baughman, A. J. Hart, *Science* **2013**, *339*, 535.
[30] J. Y. Lee, S. T. Connor, Y. Cui, P. Peumans, *Nano Lett.* **2008**, *8*, 689.
[31] P. Lee, J. Lee, H. Lee, J. Yeo, S. Hong, K. H. Nam, D. Lee, S. S. Lee, S. H. Ko, *Adv. Mater.* **2012**, *24*, 3326.
[32] F. Xu, Y. Zhu, *Adv. Mater.* **2012**, *24*, 5117.
[33] F. Bonaccorso, Z. Sun, T. Hasan, A. C. Ferrari, *Nat. Photonics* **2010**, *4*, 611.
[34] K. S. Kim, Y. Zhao, H. Jang, S. Y. Lee, J. M. Kim, K. S. Kim, J. H. Ahn, P. Kim, J. Y. Choi, B. H. Hong, *Nature* **2009**, *457*, 706.
[35] J. B. Wu, M. Agrawal, H. A. Becerril, Z. N. Bao, Z. F. Liu, Y. S. Chen, P. Peumans, *ACS Nano* **2010**, *4*, 43.
[36] H. X. Chang, G. F. Wang, A. Yang, X. M. Tao, X. Q. Liu, Y. D. Shen, Z. J. Zheng, *Adv. Funct. Mater.* **2010**, *20*, 2893.
[37] V. C. Tung, L. M. Chen, M. J. Allen, J. K. Wassei, K. Nelson, R. B. Kaner, Y. Yang, *Nano Lett.* **2009**, *9*, 1949.
[38] R. Zhu, C. H. Chung, K. C. Cha, W. B. Yang, Y. B. Zheng, H. P. Zhou, T. B. Song, C. C. Chen, P. S. Weiss, G. Li, Y. Yang, *ACS Nano* **2011**, *5*, 9877.
[39] M. S. Lee, K. Lee, S. Y. Kim, H. Lee, J. Park, K. H. Choi, H. K. Kim, D. G. Kim, D. Y. Lee, S. Nam, J. U. Park, *Nano Lett.* **2013**, *13*, 2814.
[40] Y. H. Kim, C. Sachse, M. L. Machala, C. May, L. Muller-Meskamp, K. Leo, *Adv. Funct. Mater.* **2011**, *21*, 1076.
[41] J. Holovsky, S. Nicolay, S. De Wolf, C. Ballif, *Sci. Rep.* **2015**, *5*, 15684.
[42] K. Hayashi, S. Matsuishi, T. Kamiya, M. Hirano, H. Hosono, *Nature* **2002**, *419*, 462.
[43] S. Matsuishi, Y. Toda, M. Miyakawa, K. Hayashi, T. Kamiya, M. Hirano, I. Tanaka, H. Hosono, *Science* **2003**, *301*, 626
[44] H. Hosono, M. Yasukawa, H. Kawazoe, *J. Non-Cryst. Solids* **1996**, *203*, 334.
[45] R. M. Pasquarelli, D. S. Ginley, R. O'Hayre, *Chem. Soc. Rev.* **2011**, *40*, 5406.
[46] H. Hosono, *Jpn. J. Appl. Phys.* **2013**, *52*, 9.
[47] J. E. Medvedeva, *Transparent Electronics: From Synthesis to Applications*, John Wiley & Sons, Ltd, Chichester, UK, **2010**.
[48] G. Hautier, A. Miglio, D. Waroquiers, G.-M. Rignanese, X. Gonze, *Chem. Mater.* **2014**, *26*, 5447.
[49] J. Y. W. Seto, *J. Appl. Phys.* **1975**, *46*, 5247.
[50] M. Orita, H. Ohta, M. Hirano, S. Narushima, H. Hosono, *Philos. Mag. B-Phys. Condens. Matter Stat. Mechanics Electron. Opt. Magn. Prop.* **2001**, *81*, 501.
[51] T. J. Coutts, D. L. Young, X. Li, W. P. Mulligan, X. Wu, *J. Vac. Sci. Technol. A* **2000**, *18*, 2646.
[52] K. M. Yu, M. A. Mayer, D. T. Speaks, H. C. He, R. Y. Zhao, L. Hsu, S. S. Mao, E. E. Haller, W. Walukiewicz, *J. Appl. Phys.* **2012**, *111*.
[53] E. Burstein, *Phys. Rev.* **1954**, *93*, 632.
[54] T. S. Moss, *Proc. Phys. Soc. London Sect. B* **1954**, *67*, 775.
[55] S. Trevor, G. J. B. Moss, B. Ellis, *Semiconductor Opto-Electronics*, Butterworths, London **1973**.
[56] H. Fujiwara, M. Kondo, *Phys. Rev. B* **2005**, *71*, 075109.
[57] J. I. Pankove, *Optical Processes in Semiconductors*, Dover Publications, Inc., New York, **1971**.
[58] J. Steinhauser, S. Faÿ, N. Oliveira, E. Vallat-Sauvain, C. Ballif, *Appl. Phys. Lett.* **2007**, *90*, 142107.
[59] G. Hautier, A. Miglio, G. Ceder, G. M. Rignanese, X. Gonze, *Nat. Commun.* **2013**, *4*, 2292.

[60] A. Zunger, *Appl. Phys. Lett.* **2003**, *83*, 57.
[61] H. Kawazoe, M. Yasukawa, H. Hyodo, M. Kurita, H. Yanagi, H. Hosono, *Nature* **1997**, *389*, 939.
[62] R. Nagarajan, A. D. Draeseke, A. W. Sleight, J. Tate, *Appl. Phys.* **2001**, *89*, 8022.
[63] C. Ruttanapun, W. Prachamon, A. Wichainchai, *Curr. Appl. Phys.* **2012**, *12*, 166.
[64] N. Duan, A. W. Sleight, M. K. Jayaraj, J. Tate, *J. Appl. Phys. Lett.* **2000**, *77*, 1325.
[65] R. Manoj, M. Nisha, K. A. Vanaja, M. K. Jayaraj, *Bull. Mater. Sci.* **2008**, *31*, 49.
[66] P. Mandal, N. Mazumder, S. Saha, U. K. Ghorai, R. Roy, G. C. Das, K. K. Chattopadhyay, *J. Phys. D-Appl. Phys.* **2016**, *49*, 27.
[67] L. Farrell, E. Norton, C. M. Smith, D. Caffrey, I. V. Shvets, K. Fleischer, *J. Mater. Chem. C* **2016**, *4*, 126.
[68] C. F. Windisch, G. J. Exarhos, K. F. Ferris, M. H. Engelhard, D. C. Stewart, *Thin Solid Films* **2001**, *398*, 45.
[69] P. F. Ndione, Y. Z. Shi, V. Stevanovic, S. Lany, A. Zakutayev, P. A. Parilla, J. D. Perkins, J. J. Berry, D. S. Ginley, M. F. Toney, *Adv. Funct. Mater.* **2014**, *24*, 610.
[70] W. Huang, R. Nechache, S. Li, M. Chaker, F. Rosei, *J. Am. Ceram. Soc.* **2016**, *99*, 226.
[71] K. H. L. Zhang, Y. G. Du, A. Papadogianni, O. Bierwagen, S. Sallis, L. F. J. Piper, M. E. Bowden, V. Shutthanandan, P. V. Sushko, S. A. Chambers, *Adv. Mater.* **2015**, *27*, 5191.
[72] S. Narushima, H. Mizoguchi, K. Shimizu, K. Ueda, H. Ohta, M. Hirano, T. Kamiya, H. Hosono, *Adv. Mater.* **2003**, *15*, 1409.
[73] H. Y. Chen, H. C. Su, C. H. Chen, K. L. Liu, C. M. Tsai, S. J. Yen, T. R. Yew, *J. Mater. Chem.* **2011**, *21*, 5745.
[74] E. Arca, K. Fleischer, I. V. Shvets, *Appl. Phys. Lett.* **2011**, *99*, 111910.
[75] A. Bhatia, G. Hautier, T. Nilgianskul, A. Miglio, J. Y. Sun, H. J. Kim, K. H. Kim, S. Chen, G. M. Rignanese, X. Gonze, J. Suntivich, *Chem. Mater.* **2016**, *28*, 30.
[76] C. Yang, M. Kneiss, M. Lorenz, M. Grundmann, *Proc. Natl. Acad. Sci. USA* **2016**, *113*, 12929.
[77] M. Grundmann, *Phys. Status Solidi a* **2015**, *212*, 1409.
[78] J. Varley, A. Miglio, V. A. Ha, M. J. van Setten, G.-M. Rignanese, G. Hautier, *Chem. Mater.* **2017**, DOI: 10.1021/acs.chemmater.6b04663.
[79] H. Yanagi, J. Tate, S. Park, C. H. Park, D. A. Keszler, *Appl. Phys. Lett.* **2003**, *82*, 2814.
[80] M. L. Liu, F. Q. Huang, L. D. Chen, Y. M. Wang, Y. H. Wang, G. F. Li, Q. Zhang, *Appl. Phys. Lett.* **2007**, *90*, 072109.
[81] X. J. Xu, J. Bullock, L. T. Schelhas, E. Z. Stutz, J. J. Fonseca, M. Hettick, V. L. Pool, K. F. Tai, M. F. Toney, X. S. Fang, A. Javey, L. H. Wong, J. W. Ager, *Nano Lett.* **2016**, *16*, 1925.
[82] R. Woods-Robinson, J. K. Cooper, X. J. Xu, L. T. Schelhas, V. L. Pool, A. Faghaninia, C. S. Lo, M. F. Toney, I. D. Sharp, J. W. Ager, *Adv. Electron. Mater.* **2016**, *2*, 1500396.
[83] H. Hiramatsu, K. Ueda, H. Ohta, M. Hirano, T. Kamiya, H. Hosono, *Appl. Phys. Lett.* **2003**, *82*, 1048.
[84] H. Hiramatsu, H. Yanagi, T. Kamiya, K. Ueda, M. Hirano, H. Hosono, *Chem. Mater.* **2008**, *20*, 326.
[85] J. D. Perkins, T. R. Paudel, A. Zakutayev, P. F. Ndione, P. A. Parilla, D. L. Young, S. Lany, D. S. Ginley, A. Zunger, N. H. Perry, Y. Tang, M. Grayson, T. O. Mason, J. S. Bettinger, Y. Shi, M. F. Toney, *Phys. Rev. B* **2011**, *84*, 205207.
[86] H. W. Peng, A. Zakutayev, S. Lany, T. R. Paudel, M. d'Avezac, P. F. Ndione, J. D. Perkins, D. S. Ginley, A. R. Nagaraja, N. H. Perry, T. O. Mason, A. Zunger, *Adv. Funct. Mater.* **2013**, *23*, 5267.
[87] B. A. D. Williamson, J. Buckeridge, J. Brown, S. Ansbro, R. G. Palgrave, D. O. Scanlon, *Chem. Mater.* **2016**. DOI: 10.1021/acs.chemmater.6b03306.
[88] E. C. Garnett, W. S. Cai, J. J. Cha, F. Mahmood, S. T. Connor, M. G. Christoforo, Y. Cui, M. D. McGehee, M. L. Brongersma, *Nat. Mater.* **2012**, *11*, 241.
[89] K. Zilberberg, T. Riedl, *J. Mater. Chem. A* **2016**, *4*, 14481.
[90] J. Y. Lee, S. T. Connor, Y. Cui, P. Peumans, *Nano Lett.* **2010**, *10*, 1276.
[91] C. D. Bailie, M. G. Christoforo, J. P. Mailoa, A. R. Bowring, E. L. Unger, W. H. Nguyen, J. Burschka, N. Pellet, J. Z. Lee, M. Gratzel, R. Noufi, T. Buonassisi, A. Salleo, M. D. McGehee, *Energy Environ. Sci.* **2015**, *8*, 956.
[92] D. Y. Choi, H. W. Kang, H. J. Sung, S. S. Kim, *Nanoscale* **2013**, *5*, 977.
[93] H. Lee, M. Kim, I. Kim, H. Lee, *Adv. Mater.* **2016**, *28*, 4541.
[94] K. Zilberberg, F. Gasse, R. Pagui, A. Polywka, A. Behrendt, S. Trost, R. Heiderhoff, P. Gorrn, T. Riedl, *Adv. Funct. Mater.* **2014**, *24*, 1671.
[95] T. M. Barnes, M. O. Reese, J. D. Bergeson, B. A. Larsen, J. L. Blackburn, M. C. Beard, J. Bult, J. van de Lagemaat, *Adv. Energy Mater.* **2012**, *2*, 353.
[96] M. Layani, M. Gruchko, O. Milo, I. Balberg, D. Azulay, S. Magdassi, *ACS Nano* **2009**, *3*, 3537.
[97] R. Saive, A. M. Borsuk, H. S. Emmer, C. R. Bukowsky, J. V. Lloyd, S. Yalamanchili, H. A. Atwater, *Adv. Opt. Mater.* **2016**, *4*, 1470.
[98] A. K. Geim, *Science* **2009**, *324*, 1530.
[99] J. K. Wassei, R. B. Kaner, *Mater. Today* **2010**, *13*, 52.
[100] K. S. Novoselov, V. I. Fal'ko, L. Colombo, P. R. Gellert, M. G. Schwab, K. Kim, *Nature* **2012**, *490*, 192.
[101] A. Zurutuza, C. Marinelli, *Nat. Nanotechnol.* **2014**, *9*, 730.
[102] A. Kuruvila, P. R. Kidambi, J. Kling, J. B. Wagner, J. Robertson, S. Hofmann, J. Meyer, *J. Mater. Chem. C* **2014**, *2*, 6940.
[103] W. Liu, J. H. Kang, K. Banerjee, *IEEE Electron Device Lett.* **2016**, *37*, 1246.
[104] Z. Y. Yin, S. Y. Sun, T. Salim, S. X. Wu, X. A. Huang, Q. Y. He, Y. M. Lam, H. Zhang, *ACS Nano* **2010**, *4*, 5263.
[105] H. Liu, A. T. Neal, Z. Zhu, Z. Luo, X. F. Xu, D. Tomanek, P. D. Ye, *ACS Nano* **2014**, *8*, 4033.
[106] G. R. Bhimanapati, Z. Lin, V. Meunier, Y. Jung, J. Cha, S. Das, D. Xiao, Y. Son, M. S. Strano, V. R. Cooper, L. B. Liang, S. G. Louie, E. Ringe, W. Zhou, S. S. Kim, R. R. Naik, B. G. Sumpter, H. Terrones, F. N. Xia, Y. L. Wang, J. Zhu, D. Akinwande, N. Alem, J. A. Schuller, R. E. Schaak, M. Terrones, J. A. Robinson, *ACS Nano* **2015**, *9*, 11509.
[107] Y. E. Romanyuk, H. Hagendorfer, P. Stucheli, P. Fuchs, A. R. Uhl, C. M. Sutter-Fella, M. Werner, S. Haass, J. Stuckelberger, C. Broussillou, P. P. Grand, V. Bermudez, A. N. Tiwari, *Adv. Funct. Mater.* **2015**, *25*, 12.
[108] M. Saliba, T. Matsui, J. Y. Seo, K. Domanski, J. P. Correa-Baena, M. K. Nazeeruddin, S. M. Zakeeruddin, W. Tress, A. Abate, A. Hagfeldt, M. Gratzel, *Energy Environ. Sci.* **2016**, *9*, 1989.
[109] J. Werner, L. Barraud, A. Walter, M. Bräuninger, F. Sahli, D. Sacchetto, N. Tétreault, B. Paviet-Salomon, S.-J. Moon, C. Allebé, M. Despeisse, S. Nicolay, S. De Wolf, B. Niesen, C. Ballif, *ACS Energy Lett.* **2016**, *1*, 474.
[110] Z. C. Holman, A. Descoeudres, S. De Wolf, C. Ballif, *IEEE J. Photovoltaics* **2013**, *3*, 1243.
[111] M. Morales-Masis, S. M. De Nicolas, J. Holovsky, S. De Wolf, C. Ballif, *IEEE J. Photovoltaics* **2015**, *5*, 1340.
[112] S. Albrecht, M. Saliba, J. P. C. Baena, F. Lang, L. Kegelmann, M. Mews, L. Steier, A. Abate, J. Rappich, L. Korte, R. Schlatmann, M. K. Nazeeruddin, A. Hagfeldt, M. Gratzel, B. Rech, *Energy Environ. Sci.* **2016**, *9*, 81.
[113] F. Fu, T. Feurer, T. Jager, E. Avancini, B. Bissig, S. Yoon, S. Buecheler, A. N. Tiwari, *Nat. Commun.* **2015**, *6*, 8932.
[114] T. P. White, N. N. Lal, K. R. Catchpole, *IEEE J. Photovoltaics* **2014**, *4*, 208.

[115] M. Filipic, P. Loper, B. Niesen, S. De Wolf, J. Krc, C. Ballif, M. Topic, *Opt. Express* **2015**, *23*, A263.
[116] T. Koida, H. Shibata, M. Kondo, K. Tsutsumi, A. Sakaguchi, M. Suzuki, H. Fujiwara, *J. Appl. Phys.* **2012**, *111*, 063721.
[117] E. Kobayashi, Y. Watabe, T. Yamamoto, Y. Yamada, *Sol. Energy Mater. Sol. Cells* **2016**, *149*, 75.
[118] B. Macco, H. C. M. Knoops, W. M. M. Kessels, *ACS Appl. Mater. Interfaces* **2015**, *7*, 16723.
[119] H. F. Wardenga, M. V. Frischbier, M. Morales-Masis, A. Klein, *Materials* **2015**, *8*, 561.
[120] T. Koida, H. Fujiwara, M. Kondo, *Sol. Energy Mater. Sol. Cells* **2009**, *93*, 851.
[121] L. Barraud, Z. C. Holman, N. Badel, P. Reiss, A. Descoeudres, C. Battaglia, S. De Wolf, C. Ballif, *Sol. Energy Mater. Sol. Cells* **2013**, *115*, 151.
[122] F. Y. Meng, J. H. Shi, Z. X. Liu, Y. F. Cui, Z. D. Lu, Z. Q. Feng, *Sol. Energy Mater. Sol. Cells* **2014**, *122*, 70.
[123] T. Jager, Y. E. Romanyuk, S. Nishiwaki, B. Bissig, F. Pianezzi, P. Fuchs, C. Gretener, M. Dobeli, A. N. Tiwari, *J. Appl. Phys.* **2015**, *117*, 205301.
[124] J. Werner, C. H. Weng, A. Walter, L. Fesquet, J. P. Seif, S. De Wolf, B. Niesen, C. Ballif, *J. Phys. Chem. Lett.* **2016**, *7*, 161.
[125] M. P. Taylor, D. W. Readey, M. F.A. M. van Hest, C. W. Teplin, J. L. Alleman, M. S. Dabney, L. M. Gedvilas, B. M. Keyes, B. To, J. D. Perkins, D. S. Ginley, *Adv. Funct. Mater.* **2008**, *18*, 3169.
[126] A. J. Leenheer, J. D. Perkins, M. F.A. M. van Hest, J. J. Berry, R. P. O'Hayre, D. S. Ginley, *Phys. Rev. B* **2008**, *77*, 115215.
[127] F. Urbach, *Phys. Rev.* **1953**, *92*, 1324.
[128] S. John, C. Soukoulis, M. H. Cohen, E. N. Economou, *Phys. Rev. Lett.* **1986**, *57*, 1777.
[129] W. Korner, P. Gumbsch, C. Elsasser, *Phys. Rev. B*, *86*, 5.
[130] J. Werner, G. Dubuis, A. Walter, P. Löper, S.-J. Moon, S. Nicolay, M. Morales-Masis, S. De Wolf, B. Niesen, C. Ballif, *Sol. Energy Mater. Sol. Cells* **2015**, *141*, 407.
[131] K. Ellmer, *J. Phys. D* **2001**, *34*, 3097.
[132] W. W. Wenas, A. Yamada, K. Takahashi, M. Yoshino, M. Konagai, *J. Appl. Phys.* **1991**, *70*, 7119.
[133] S. Fay, J. Steinhauser, N. Oliveira, E. Vallat-Sauvain, C. Ballif, *Thin Solid Films* **2007**, *515*, 8558.
[134] L. Fanni, A. B. Aebersold, M. Morales-Masis, D. T. L. Alexander, A. Hessler-Wyser, S. Nicolay, C. Hebert, C. Ballif, *Cryst. Growth Des.* **2015**, *15*, 5886.
[135] S. Fay, L. Feitknecht, R. Schluchter, U. Kroll, E. Vallat-Sauvain, A. Shah, *Sol. Energy Mater. Sol. Cells* **2006**, *90*, 2960.
[136] L. Ding, S. Nicolay, J. Steinhauser, U. Kroll, C. Ballif, *Adv. Funct. Mater.* **2013**, *23*, 5177.
[137] L. Ding, L. Fanni, D. Messerschmidt, S. Zabihzadeh, M. M. Masis, S. Nicolay, C. Ballif, *Sol. Energy Mater. Sol. Cells* **2014**, *128*, 378.
[138] S. Nicolay, M. Benkhaira, L. Ding, J. Escarre, G. Bugnon, F. Meillaud, C. Ballif, *Sol. Energy Mater. Sol. Cells* **2012**, *105*, 46.
[139] T. Kobayashi, K. Yamauchi, T. Nakada, *IEEE J. Photovoltaics* **2013**, *3*, 1079.
[140] P. Loper, S. J. Moon, S. M. de Nicolas, B. Niesen, M. Ledinsky, S. Nicolay, J. Bailat, J. H. Yum, S. De Wolf, C. Ballif, *Phys. Chem. Chem. Phys.* **2015**, *17*, 1619.
[141] Z. C. Holman, M. Filipic, A. Descoeudres, S. De Wolf, F. Smole, M. Topic, C. Ballif, *J. Appl. Phys.* **2013**, *113*, 013107.
[142] K. Suzuki, *Thin Solid Films* **1999**, *351*, 8.
[143] G. Brauer, *Surf. Coat. Technol.* **1999**, *112*, 358.
[144] M. Berginski, J. Hupkes, M. Schulte, G. Schope, H. Stiebig, B. Rech, M. Wuttig, *Appl. Phys.* **2007**, *101*, 074903.
[145] A. Dabirian, S. M. de Nicolas, B. Niesen, A. Hessler-Wyser, S. De Wolf, M. Morales-Masis, C. Ballif, *Adv. Mater. Interfaces* **2016**, *3*, 1500462.
[146] R. G. Gordon, *MRS Bull.* **2000**, *25*, 52.
[147] A. Lyubchyk, A. Vicente, B. Soule, P. U. Alves, T. Mateus, M. J. Mendes, H. Aguas, E. Fortunato, R. Martins, *Adv. Electron. Mater.* **2016**, *2*, 1500287.
[148] F. Ruske, M. Roczen, K. Lee, M. Wimmer, S. Gall, J. Hupkes, D. Hrunski, B. Rech, *J. Appl. Phys.* **2010**, *107*, 013708.
[149] H. Hagendorfer, K. Lienau, S. Nishiwaki, C. M. Fella, L. Kranz, A. R. Uhl, D. Jaeger, L. Luo, C. Gretener, S. Buecheler, Y. E. Romanyuk, A. N. Tiwari, *Adv. Mater.* **2014**, *26*, 632.
[150] C. Guillen, J. Herrero, *Thin Solid Films* **2011**, *520*, 1.
[151] W. Wang, M. Song, T. S. Bae, Y. H. Park, Y. C. Kang, S. G. Lee, S. Y. Kim, D. H. Kim, S. Lee, G. H. Min, G. H. Lee, J. W. Kang, J. Yun, *Adv. Funct. Mater.* **2014**, *24*, 1551.
[152] N. P. Sergeant, A. Hadipour, B. Niesen, D. Cheyns, P. Heremans, P. Peumans, B. P. Rand, *Adv. Mater.* **2012**, *24*, 728.
[153] L. Cattin, J. C. Bernede, M. Morsli, *Phys. Status Solidi a* **2013**, *210*, 1047.
[154] Graphene Supermarket, https://graphene-supermarket.com, accessed October 2016.
[155] Fluxim Setfos simulation software, www.fluxim.com, accessed October 2016.
[156] F. Dauzou, P. C. P. Bouten, A. Dabirian, Y. Leterrier, C. Ballif, M. Morales-Masis, *Org. Electron.* **2016**, *35*, 136.
[157] M. Morales-Masis, F. Dauzou, Q. Jeangros, A. Dabirian, H. Lifka, R. Gierth, M. Ruske, D. Moet, A. Hessler-Wyser, C. Ballif, *Adv. Funct. Mater.* **2016**, *26*, 384.
[158] M. R. Krames, O. B. Shchekin, R. Mueller-Mach, G. O. Mueller, L. Zhou, G. Harbers, M. G. Craford, *J. Display Technol.* **2007**, *3*, 160.
[159] N. Weiss, L. Muller-Meskamp, F. Selzer, L. Bormann, A. Eychmuller, K. Leo, N. Gaponik, *RSC Adv.* **2015**, *5*, 19659.
[160] L. B. Hu, H. S. Kim, J. Y. Lee, P. Peumans, Y. Cui, *ACS Nano* **2010**, *4*, 2955.
[161] Y. Lee, S.-Y. Min, T.-S. Kim, S.-H. Jeong, J. Y. Won, H. Kim, W. Xu, J. K. Jeong, T.-W. Lee, *Adv. Mater.* **2016**, *28*, 9109.
[162] J. Meyer, P. R. Kidambi, B. C. Bayer, C. Weijtens, A. Kuhn, A. Centeno, A. Pesquera, A. Zurutuza, J. Robertson, S. Hofmann, *Sci. Rep.* **2014**, *4*, 5380.
[163] N. Li, S. Oida, G. S. Tulevski, S. J. Han, J. B. Hannon, D. K. Sadana, T. C. Chen, *Nat. Commun.* **2013**, *4*, 2294.
[164] S. De Wolf, M. Kondo, *J. Appl. Phys.* **2009**, *105*, 103707.
[165] A. Dualeh, N. Tetreault, T. Moehl, P. Gao, M. K. Nazeeruddin, M. Gratzel, *Adv. Funct. Mater.* **2014**, *24*, 3250.
[166] E. Shanthi, A. Banerjee, V. Dutta, K. L. Chopra, *J. Appl. Phys.* **1982**, *53*, 1615.
[167] B. Stjerna, E. Olsson, C. G. Granqvist, *J. Appl. Phys.* **1994**, *76*, 3797.
[168] H. Kim, R. C. Y. Auyeung, A. Pique, *Thin Solid Films* **2008**, *516*, 5052.
[169] J. Werner, J. Geisskihler, A. Dabirian, S. Nicolay, M. Morales-Masis, S. De Wolf, B. Niesen, C. Ballif, *ACS Appl. Mater. Interfaces* **2016**, *8*, 17260.
[170] S. J. Wakeham, M. J. Thwaites, B. W. Holton, C. Tsakonas, W. M. Cranton, D. C. Koutsogeorgis, R. Ranson, *Thin Solid Films* **2009**, *518*, 1355.
[171] B. Demaurex, J. P. Seif, S. Smit, B. Macco, W. M. M. Kessels, J. Geissbuhler, S. De Wolf, C. Ballif, *IEEE J. Photovoltaics* **2014**, *4*, 1387.
[172] K. Zilberberg, J. Meyer, T. Riedl, *J. Mater. Chem. C* **2013**, *1*, 4796.
[173] A. Kanevce, W. K. Metzger, *J. Appl. Phys.* **2009**, *105*, 094507.
[174] L. J. Brillson, Y. C. Lu, *J. Appl. Phys.* **2011**, *109*, 121301.
[175] D. K. Schroder, D. L. Meier, *IEEE Trans. Electron Devices* **1984**, *31*, 637.

[176] J. Geissbuhler, S. De Wolf, A. Faes, N. Badel, Q. Jeangros, A. Tomasi, L. Barraud, A. Descoeudres, M. Despeisse, C. Ballif, *IEEE J. Photovoltaics* **2014**, *4*, 1055.
[177] C. G. Tang, M. C. Y. Ang, K.-K. Choo, V. Keerthi, J.-K. Tan, M. N. Syafiqah, T. Kugler, J. H. Burroughes, R.-Q. Png, L.-L. Chua, P. K. H. Ho, *Nature* **2016**, *539*, 536.
[178] G. Nogay, J. P. Seif, Y. Riesen, A. Tomasi, Q. Jeangros, N. Wyrsch, F. J. Haug, S. De Wolf, C. Ballif, *IEEE J. Photovoltaics* **2016**, *6*, 1654.
[179] M. G. Helander, Z. B. Wang, J. Qiu, M. T. Greiner, D. P. Puzzo, Z. W. Liu, Z. H. Lu, *Science* **2011**, *332*, 944.
[180] T. C. Yeh, Q. Zhu, D. B. Buchholz, A. B. Martinson, R. P. H. Chang, T. O. Mason, *Appl. Surf. Sci.* **2015**, *330*, 405.
[181] M. T. Greiner, Z. H. Lu, *NPG Asia Mater.* **2013**, *5*, e55.
[182] J. Meyer, S. Hamwi, M. Kroger, W. Kowalsky, T. Riedl, A. Kahn, *Adv. Mater.* **2012**, *24*, 5408.
[183] T. Tohsophon, A. Dabirian, S. De Wolf, M. Morales-Masis, C. Ballif, *APL Mater.* **2015**, *3*, 116105.
[184] T. Tohsophon, J. Hupkes, S. Calnan, W. Reetz, B. Rech, W. Beyer, N. Sirikulrat, *Thin Solid Films* **2006**, *511*, 673.
[185] T. Koida, *Phys. Status Solidi a* **2016**, *214*, 1600464.
[186] J. Werner, A. Walter, E. Rucavado, S.-J. Moon, D. Sacchetto, M. Rienaecker, R. Peibst, R. Brendel, X. Niquille, S. De Wolf, P. Löper, M. Morales-Masis, S. Nicolay, B. Niesen, C. Ballif, *Appl. Phys. Lett.* **2016**, *109*, 233902.
[187] D. Cheneler, J. Bowen, *Soft Matter* **2013**, *9*, 344.
[188] Y. Shigesato, S. Takaki, T. Haranoh, *J. Appl. Phys.* **1992**, *71*, 3356.
[189] K. Iwata, T. Sakemi, A. Yamada, R. Fons, K. Awai, I. Yamamoto, M. Matsubara, H. Tampo, K. Sakurai, S. Ishizuka, S. Niki, *Thin Solid Films* **2004**, *451*, 219.
[190] Y. Hoshi, H. Kato, K. Funatsu, *Thin Solid Films* **2003**, *445*, 245.
[191] M. Hamedi, R. Forchheimer, O. Inganas, *Nat. Mater.* **2007**, *6*, 357.
[192] R. F. Service, *Science* **2003**, *301*, 909.

